AMERICAN JOURNAL OF PHYSICAL ANTHROPOLOGY 116:108–139 (2001)

# In Vivo Function of the Craniofacial Haft: The Interorbital "Pillar"

Callum F. Ross*

*Anatomical Sciences, Health Sciences Center, SUNY at Stony Brook, Stony Brook, NY 11794-8081*

*KEY WORDS* primates; bone strain; mastication; biomechanics; evolution

*ABSTRACT* The craniofacial haft resists forces generated in the face during feeding, but the importance of these forces for the form of the craniofacial haft remains to be determined. In vivo bone strain data were recorded from the medial orbital wall in an owl monkey (*Aotus*), rhesus macaques (*Macaca mulatta*), and a galago (*Otolemur*) during feeding. These data were used to determine whether: the interorbital region can be modeled as a simple beam under bending or shear; the face is twisting on the brain case during unilateral biting or mastication; the interorbital "pillar" is being axially compressed during incisor loading and both axially compressed and laterally bent during mastication; and the interorbital "pillar" transmits axial compressive forces from the toothrow to the braincase.

The strain data reveal that the interorbital region cannot be modeled as a anteroposteriorly oriented beam bent superiorly in the sagittal plane during incision or mastication. The strain orientations recorded in the majority of experiments are concordant with those predicted for a short beam under shear, although the anthropoids displayed evidence of multiple loading regimes in the medial orbital wall. Strain orientation data corroborate the hypothesis that the strepsirrhine face is twisted during mastication. The hypothesis that the interorbital region is a member in a rigid frame subjected to axial compression during mastication receives some support. The hypothesis that the interorbital region is a member in a rigid frame subjected to lateral bending during mastication is supported by the $\epsilon_1/|\epsilon_2|$ ratio data but not by the strain orientation data. The timing of peak shear strains in the medial orbital wall of anthropoids does not bear a consistent relationship to the timing of peak shear strain in the mandibular corpus, suggesting that bite force is not the only external force influencing the medial orbital wall. Strain orientation data suggest the existence of two distinct loading regimes, possibly associated with masseter or medial pterygoid contraction. Regardless of the loading regime, all taxa showed low strain magnitudes in the medial orbital wall relative to the anterior root of the zygoma and the mandibular corpus. The strain gradients documented here and elsewhere suggest that, in anthropoids at least, local effects of external forces are more important than a single global loading regime. The low strain magnitudes in the medial orbital wall and in other thin bony plates around the orbit suggest that these structures are not optimally designed for resisting feeding forces. It is hypothesized that their function is to provide rigid support and protection for soft-tissue structures such as the nasal epithelium, the brain, meninges, and the eye and its adnexa. In contrast with the face of *Otolemur*, which appears to be subjected to a single predominant loading regime, anthropoids may experience different loading regimes in different parts of the face. This implies that the anthropoid and strepsirrhine facial skulls might be optimized for different functions. Am J Phys Anthropol 116:108–139, 2001. 

Forces generated in the vertebrate face during feeding must be resisted by the skull. Many fishes, snakes, birds, and lizards have highly kinetic skulls which absorb these forces through movement and in elastic tissues of the bones or joints (Frazetta, 1962; Zusi, 1984; Schwenk, 2000). Even some mammals (e.g., pigs, Herring and Mucci, 1991; Herring and Teng, 2000) have mobile, patent sutures that might serve similar functions. However, mammals (like crocodylians) have akinetic skulls in which the face does not move relative to the brain case during feeding. Consequently, any external moments acting on the mammalian face that are not resisted by other external moments must be resisted by (and produce stress in) the bony connections between the face and brain case: the craniofacial haft. Various hypotheses regarding the loading regimes in the faces of primates, particularly humans, have been advanced. Several of these hypotheses are evaluated here.

## IS THE PRIMATE INTERORBITAL REGION A BENDING BEAM?

One of the aims of the research reported here is to determine whether the interorbital region of primates can be modeled as an anteroposteriorly oriented beam (Fig. 1). Many hypotheses have modeled

Grant sponsor: NSF; Grant number: 9706676.

*Correspondence to: Callum F. Ross, Anatomical Sciences, Health Sciences Center, SUNY at Stony Brook, Stony Brook, NY 11794-8081. E-mail: cross@mail.som.sunysb.edu

Received 1 December 2000; accepted 22 June 2001.

the face or parts of the face as a single unit structure (i.e., a beam or cylinder) subjected to varying amounts of bending, compression, shear, and twisting (e.g., Greaves, 1985; Thomason and Russell, 1986; Preuschoft et al., 1986). These beam models of the rostrum, face, or whole skull (Preuschoft et al., 1986; Russell and Thomason, 1993; Greaves, 1985, 1995) have been contradicted by cross-sectional geometry, and morphometric and in vivo strain gauge data (Demes, 1982; Preuschoft et al., 1986; Ravosa, 1988; 1991; Hylander et al., 1991; Ross and Hylander, 1996). These models are probably inaccurate because with increasing scale, the external forces acting on the skull become more diverse in relative magnitude, orientation, and point of application; skull morphology deviates progressively from that of a simple beam or cylinder; and there is an increasing heterogeneity of the material properties of bone and sutures (Dechow et al., 1993; Herring and Mucci, 1991; Jaslow, 1990; Rafferty and Herring, 2000). In contrast to these large-scale beam models, more simple beam or plate models of the zygomatic arch, mandibular corpus, mandibular symphysis, and postorbital septum have been corroborated by in vivo data, comparative morphometrics, and finite-element models (Hylander, 1979a,b, 1981, 1985; Borrazo et al., 1994; Herring et al., 1996; Ross and Hylander 1996; Ross and Chen, 1997; Hylander and Johnson, 1997). Beam models of parts of the primate face appear to be useful when the parts of the face modeled as beams approximate the dimensions of a beam or other simple structure, when they are loaded by only a small number of external forces or one predominant force at a time, and when the area modeled possesses relatively homogeneous material properties.

Can the interorbital region be modeled as a beam? In support of this possibility, in the frontal plane the primate circumorbital region resembles a cross section through an I-beam, with the interorbital "pillar" corresponding to the vertical web and the supraorbital torus and palate forming the upper and lower

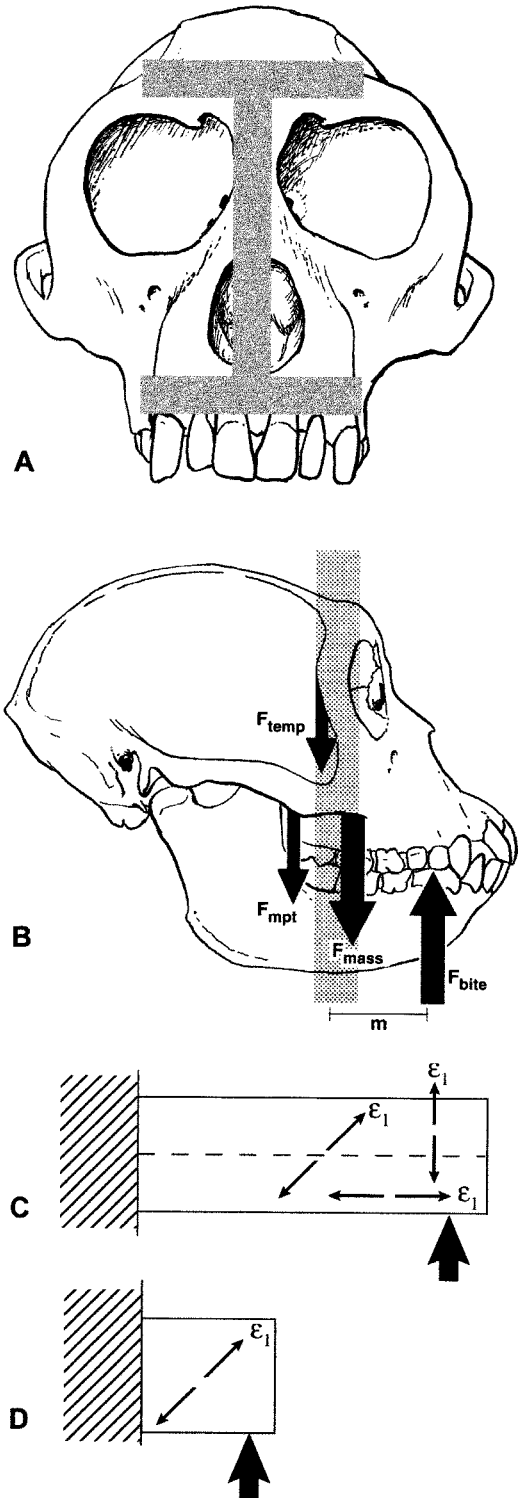


**Fig. 1. A:** Macaque skull with cross section of an I-beam superimposed, illustrating gross similarity between cross section of macaque facial region and an I-beam. This is not meant to imply that the shape of the macaque face is an *adaptation* to resist bending in sagittal planes, although the shape of the face does make it strong under bending. **B:** Important external forces acting on the face during feeding. $F_{temp}$, inferiorly directed component of temporalis muscle force acting on lateral orbital wall; $F_{mass}$, inferiorly directed component of masseter muscle force acting on anterior root of zygomatic arch; $F_{mpt}$, inferiorly directed component of medial pterygoid muscle force acting on pterygoid process of sphenoid bone; $F_{bite}$, superiorly directed component of bite force acting on tooth row. Stippled zone indicates cross sections in which intraorbital strain gauges were placed. Any frontal plane of the face will be subjected to superiorly directed bending and shearing moments when the superiorly directed components of bite force ($F_{bite}$) exceed the inferiorly directed components of muscle force acting anterior to that plane. Therefore, anterior to the insertion of masseter, the face must be subjected to superiorly directed bending and shearing moments during feeding. Frontal planes in the circumorbital region, indicated by the zone of stipple, will also be subjected to superiorly directed bending and shearing moments when $F_{bite} * m > F_{mass} + F_{temp}$ (assuming the moment arms of the muscle forces are negligible). As argued in the text, $F_{bite} * m$ is probably always greater than $F_{mass} + F_{temp}$ during mastication and incision. **C:** Pattern of strain ($\varepsilon_1$ orientation only) on the lateral surface of a long beam subjected to a superiorly directed moment. **D:** Pattern of strain ($\varepsilon_1$ orientation only) on the lateral surface of a short beam subjected to a superiorly directed moment.

flanges (Fig. 1A). The vertical orientation and relatively flat shape of the medial orbital walls of anthropoids and many strepsirrhines might correspond to the sides of an I-beam. It is also noteworthy that the medial orbital walls of most primates do not give origin to muscles of mastication, so that local (Saint-Venant's) effects of muscle contraction might not influence loading regimes in this region.

The hypothesis of beam-like behavior of the interorbital region is evaluated here. How is this interorbital "beam" loaded during feeding? Probably the largest single force acting on the face during feeding is the superiorly[1] directed component of bite force acting on the tooth row ($F_{bite}$, Fig. 1B). When this force acts at any point rostral to the insertions of the masticatory muscles there are no ventrally directed forces available to counter it, and the face must be subjected to superiorly directed bending moments and associated shearing forces (Görke, 1904; Endo, 1966; Hylander, 1972, 1977; Cartmill, 1974; Demes, 1982; Rak, 1983; Preuschoft et al., 1986). In addition, superiorly directed bending moments and shearing forces will act in more posterior planes in which the moments due to the superiorly directed bite force ($F_{bite}$) exceed those due to the inferiorly directed muscle forces ($F_{mass}$, $F_{mpt}$, $F_{temp}$, Fig. 1B). This is likely to be the case for the majority of the medial orbital wall, because the bite force receives contributions from the temporalis and medial pterygoid, as well as masseter, so that the bending moments acting on the interorbital region due to the bite force probably always exceed the oppositely directed moments due to masseter contraction.

It is therefore hypothesized that the interorbital "beam" is subjected to a superiorly directed bending moment during incision. Bending moments acting on the interorbital region will be greatest during incision, when the moment arm of the bite force is longest. However, as the line of action of the superiorly directed component of bite force moves posteriorly, these bending moments will decrease in importance relative to shearing forces. In short beams, i.e., beams with their length less than four times their diameter, stress due to shear is more important than stress due to bending (Roark and Young, 1975, p. 184–188). As the beam becomes shorter, with span/depth ratios approaching 1, stresses (including those due to shear) can become very large indeed (Roark and Young, 1975, p. 186). Because the primate interorbital region is a short beam, if it is a beam at all, and because the molar tooth row lies below the orbit in the species examined here (indeed, in all primates), shear stresses are predicted to be more important than bending moments in the primate interorbital region during mastication.

[1]Inferior refers to the bottom of the skull, i.e., the inferior edge of the mandible, superior refers to the opposite direction, anterior towards the tip of the snout, and posterior towards the nuchal region.

Thus, it is hypothesized that the interorbital "beam" will be subjected to bending moments and shearing forces during incision, and to predominantly shearing forces during mastication and molar biting. If the interorbital region is behaving as a bending cantilever beam during incision, the maximum principal strain orientations shown in Figure 1C are predicted. Maximum principal strain orientations should be antero-posterior above the bending axis of neutrality, supero-inferior below it, and oblique to the axis right on the axis itself. If the face is behaving as a short beam under shear during mastication, the maximum principal strain orientations shown in Figure 1D are predicted on and near the central axis, with shear strain and stress decreasing away from the central axis of the beam (Hibbeler, 1997, p. 367).

## IS THE PRIMATE FACE A TWISTING CYLINDER?

The second aim of this research is to determine whether the strepsirrhine face is behaving like a simple cylinder subjected to torsion (Greaves, 1985; Rak, 1986). Greaves (1985) hypothesized that during mastication, the mammalian skull behaves like a cylinder that is twisted about an anteroposterior axis. Greaves (1985) postulated that the unilaterally acting, superiorly directed bite force exerts a torque on the face, twisting it on the brain case. This hypothesis has received only mixed support (Hylander et al., 1991; Ross and Hylander, 1996; Ravosa et al., 2000a,b; Herring and Teng, 2000), with the most compelling support coming from in vivo bone strain recordings from the dorsal interorbital region and postorbital bar of galagos (Ravosa et al., 2000b). Here, further evidence in support of this hypothesis is presented from the medial orbital wall of galagos. For completeness, this hypothesis is also evaluated for the anthropoids examined here.

The pattern of strain predicted by this hypothesis has been presented in detail elsewhere (Hylander et al., 1991; Ross and Hylander, 1996; Ravosa et al., 2000b), and is only summarized here. In a solid cylinder under torsion, maximum principal (tensile) strains are oriented obliquely along the cylinder in the direction of the torque, at 45° to the twisting axis (Fig. 2A). Reversal of the torque direction causes a 90° rotation of the orientation of the principal strains (Fig. 2B). Because the orientation of the twisting axis in the primate face is unknown, this hypothesis cannot be precisely evaluated using strain orientation data. However, the 90° rotation of the orientation of the principal strains with changes in chewing side is a testable prediction.

## IS THE PRIMATE INTERORBITAL REGION PART OF A RIGID FRAME SUBJECTED TO AXIAL COMPRESSIVE FORCES AND BENDING MOMENTS?

A third aim of the research reported here is to determine whether the interorbital region behaves

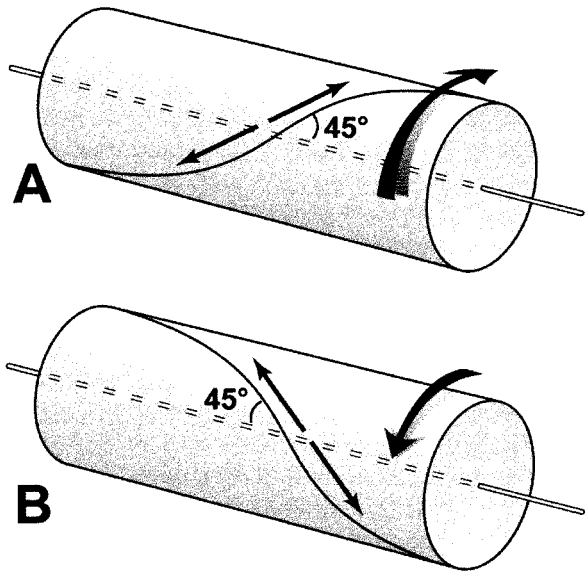


**Fig. 2.** Diagram illustrating $\varepsilon_1$ orientations (arrows) predicted for solid cylinders under pure torsion. A clockwise twist (shown in top cylinder) produces $\varepsilon_1$ orientations superior and forward at 45° to the long axis of the cylinder, as shown. A counterclockwise twist (shown in bottom cylinder) produces $\varepsilon_1$ orientations downward and forward at 45° to the long axis of the cylinder, as shown.

as predicted by the rigid frame model of the primate face by Endo (1966). Several workers have posited that the primate face can be modeled as a rigid frame composed of several straight elements (e.g., Görke, 1904; Richter, 1920; Bluntschli, 1926; Sicher and Tandler, 1928; Endo, 1966; Roberts and Tattersall, 1974; Couly, 1976; Rak, 1983) (Fig. 3). The most elaborate of these models is that by Endo (1966, 1970, 1973) in his classic studies of the human skull, which have influenced many students of primate craniofacial biomechanics (reviewed in Picq and Hylander, 1989). Endo's model of the facial skeleton comprises a rigid frame consisting of straight members of uniform cross section. The stresses throughout the facial frame were estimated in frontal (Fig. 3A) and lateral perspectives using a mathematical model, and the model was evaluated using in vitro strain gauge analysis of skulls of *Homo* and *Gorilla* (Endo, 1966, 1970, 1973). With some exceptions (Picq and Hylander, 1989), the patterns of stress predicted by the mathematical model are matched fairly closely by patterns of bone strain recorded under in vitro loading. In particular, patterns of stress predicted in the nasal member (the interorbital element) during incisor and molar loading corresponded closely to patterns of strain recorded during in vitro loading. These predictions are evaluated here, using in vivo bone strain data. Endo's model was derived for *Homo* and *Gorilla*, and the data reported here are from *Macaca*, *Aotus*, and *Otolemur*. The predictions of Endo's model can be evaluated in all three species if it is assumed that rigid frame models of all these taxa would include a single vertically oriented member in the interorbital region.

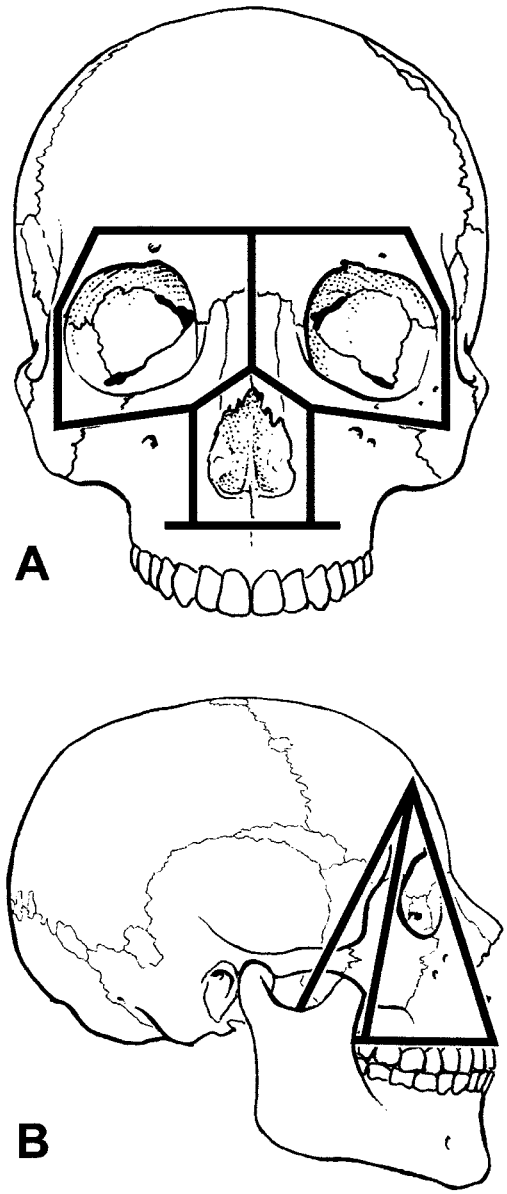


**Fig. 3.** Rigid frame models of the human face presented by (**A**) Endo (1966) and (**B**) Roberts and Tattersall (1974).

Figure 4 illustrates the rigid frame model abstracted from the macaque face in frontal (Fig. 4A) and lateral (Fig. 4B) view, with the patterns of strain predicted for incisor loading. Figure 4C illustrates the rigid frame model abstracted from the macaque face in frontal view, with the patterns of strain predicted during mastication on the right side. The rigid frame is drawn to resemble models by Endo (1966, 1970, 1973) for *Homo* and *Gorilla*.

### Incisor biting

Endo (1966) suggests that during anterior dental loading in humans and gorillas, the midline nasal member is subjected to axial compressive forces and bending moments acting in the sagittal plane. In

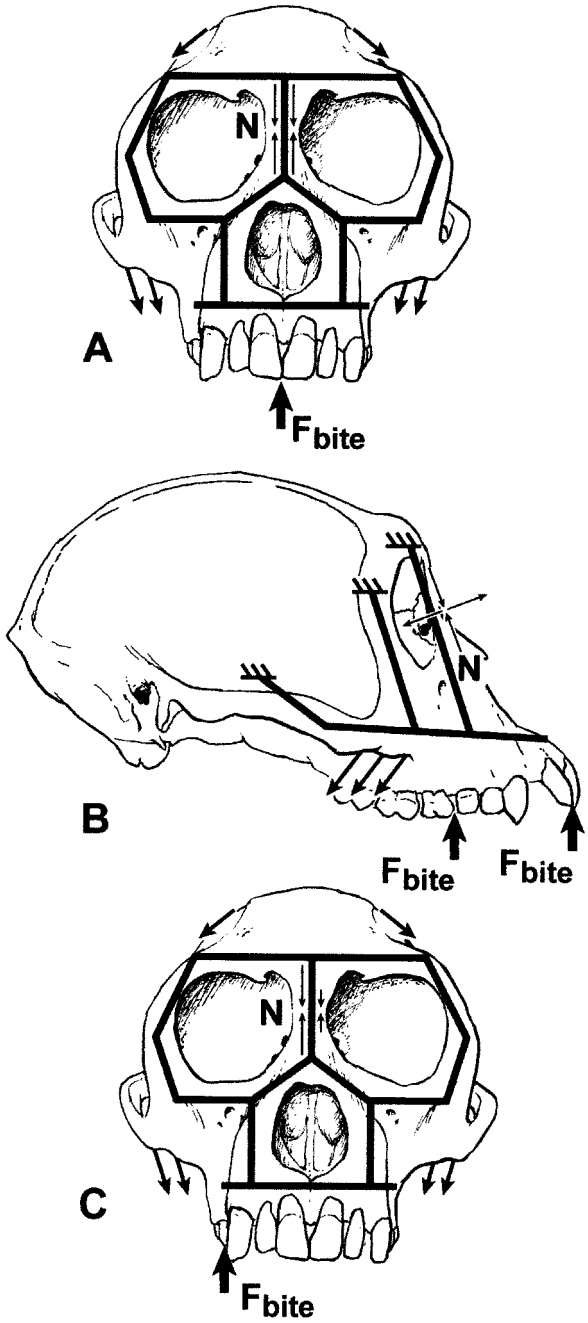


**Fig. 4.** Adaptation of rigid frame model of Endo (1966) in *Homo* and *Gorilla* to the face of *Macaca*. **A:** Frame model in frontal view, illustrating external forces acting on the frame model during incision; and strain orientations predicted in the interorbital region by Endo (1966). **B:** Frame model in lateral view, illustrating external forces acting on the frame model during incision or mastication; and strain orientations predicted in the interorbital region by Endo (1966) during either incisor biting or right sided chewing. **C:** Frame model in frontal view, illustrating external forces acting on the frame model during right-sided chewing; and strain orientations predicted in the interorbital region by Endo (1966). Arrows on either side of interorbital member (N) represent strain orientations: converging arrows indicate compressive ($\varepsilon_2$) strain orientations, and diverging arrows indicate principal tensile strain ($\varepsilon_1$) orientations. Larger arrows beneath zygomatic arches and along temporal lines represent muscle forces.

humans, the nasal member is convex anteriorly, so that anterior dental loading is accompanied by significant bending moments, whereas in *Gorilla*, the nasal member is straight, so that axial compressive forces predominate and bending moments are reduced relative to the human. The face of *Macaca* (and those of *Aotus* and *Otolemur*) resembles that of *Gorilla* in lacking the anterior convexity to the nasal region, suggesting that their interorbital regions can also be hypothesized to be subjected predominantly to axial compression, rather than bending, during anterior dental loading (i.e., incision and incisor biting). Evaluating these hypotheses requires an estimate of the orientation of the interorbital "member" in lateral view. Endo (1966) suggested that the nasal member of *Gorilla* is not vertical, but slants posteriorly, an orientation suggested here for the macaque facial frame (Fig. 4B). Under this assumption, patterns of strain predicted under incision are illustrated for *Macaca* in Figure 4A,B: tensile strains are predicted to be oriented anterosuperiorly, i.e., perpendicular to the long axis of the "nasal member." These strain orientations are plausible because they were produced by in vitro incisor loading of *Gorilla* and *Homo* skulls (Endo, 1966, 1970, 1973).

### Mastication

Endo (1966) found that during loading of the posterior tooth row, the nasal member of both humans and gorillas is subjected to both laterally directed bending moments and axial compressive forces.[2] Axial compression produces the patterns of strain illustrated in Figure 4A,B; the patterns of strain predicted by a combination of axial compression and lateral bending are illustrated in Figure 4C. On the side of the interorbital member ipsilateral to the bite force, the member will experience superoinferiorly oriented compression (and anteroposterior tension) due to the combination of axial compression and compression due to bending, and a predominance of compressive over tensile strain. Under pure bending, the side of the interorbital member contralateral to the bite point is expected to exhibit superoinferiorly oriented tension. Ross and Hylander (1996) advanced a similar model for the behavior of the face of *Aotus* during mastication. They hypothesized that during mastication, the palate "rocks" from side to side (Ross and Hylander, 1996), predicting that during mastication the working side of the interorbital pillar is dorsoventrally compressed and the balancing side is dorsoventrally tensed. However, when this bending is combined with large axial compressive forces, strain orientations might vary from those predicted for axial compression (i.e., anterosuperiorly oriented tension) to those predicted under pure bending (posterosuperiorly oriented ten-

[2]The comparisons by Endo (1966) between stress magnitudes generated by loading different parts of the tooth row are flawed (Picq and Hylander, 1989), and are not considered here.

sion), depending on the relative importance of the two loading regimes. Similarly, compressive forces on the contralateral side of the interorbital member might vary between equal to and smaller than those seen ipsilateral to the bite point. The in vitro studies by Endo (1966, 1970, 1973) of *Homo* and *Gorilla* skulls (Endo, 1966, his Fig. 3.6A,B) revealed that during molar loading, the principal compressive strains on the ipsilateral side of the interorbital member are oriented supero-inferiorly, whereas on the contralateral side of the interorbital member there is also superoinferiorly oriented compression, but of a smaller magnitude than the ipsilateral side. This prediction is illustrated in Figure 4C.

## DOES THE PRIMATE INTERORBITAL REGION TRANSMIT AXIAL COMPRESSIVE STRESSES TO THE BRAIN CASE?

A common component of the framework models, such as those of Görke (1904) and Benninghof and Goerttler (1957), is the idea that the bones of the craniofacial haft comprise vertical pillars that are primarily axially compressed during mastication and incision. The version by Roberts and Tattersall (1974) of this model posits that in humans, an anterior "member" transmits stresses from the anterior dentition to the domed frontal bone via the canine root and frontal process of the maxilla, a lateral member transmits stresses from the molar region up to the frontal bone via the postorbital bar, and a posterior member transmits stresses to the frontal via the pterygoid processes of the sphenoid and the basicranium (Fig. 3B). Tucker (1954a–f, 1955a–c) makes a similar argument, although he discriminates between mammals such as carnivores, in which the bite forces are concentrated at restricted areas of the tooth row, and primates in which the bite forces are spread across a larger area of the tooth row. Animals with concentrated bite forces are predicted by Tucker (1954a, 1955b,c) to develop structures (some of which traverse the craniofacial haft) to transmit these stresses to other parts of the skull, whereas mammals with more diffuse areas of force application will resist those stresses locally.

The degree of transmission, concentration, or dispersion of primate bite forces is currently unknown, but in vivo bone strain data from the superficial aspects of the primate craniofacial haft are relevant to the hypotheses of Roberts and Tattersall (1974) and Tucker(1954a–f, 1955a–c) regarding the primate skull. If Roberts and Tattersall (1974) are correct, axial compressive stresses should be consistently high in the interorbital and lateral orbital members of the facial framework. Assuming constant cross-sectional areas and material properties from the bottom to the top of the interorbital "pillar," Roberts and Tattersall (1974) also predicted relatively constant strains. If Tucker (1954a–f, 1955a–c) is correct, there should be strong strain gradients between the tooth row and the craniofacial haft in primates but not in carnivores.

In *Macaca*, steep strain gradients are apparent passing up the lateral orbital wall from the anterior root of the zygomatic arch to the supraorbital region (Hylander and Johnson, 1992), and in *Aotus*, *Otolemur*, and *Macaca*, strain in the supraorbital region is lower than that seen in the lateral orbital wall, which in turn is lower than that recorded simultaneously from the mandible or zygomatic arch (Hylander et al., 1991; Hylander and Johnson, 1992; Ross and Hylander, 1996; Ravosa et al., 2000a,b). These results suggest that, in primates, external forces are resisted close to the points of application (i.e., the tooth row and zygoma) and are not transmitted to the neurocranium via the craniofacial haft. Similar results have been reported for in vitro loading (Endo, 1966) and finite-element modeling (Arbel and Hershkovitz, 2000) studies of the human skull, and suggest that local effects might be more important than global loading regimes in determining primate facial form. Here the stress-transmission hypothesis is evaluated in the medial orbital wall by determining whether the strain gradients evident elsewhere in the face are also apparent in the interorbital "pillar."

## PURPOSE OF THIS INVESTIGATION

This paper evaluates these simple beam, cylinder, and framework models of the primate face, using in vivo bone strain data from the medial orbital walls of three primate species: *Macaca mulatta*, *Aotus* sp.?, and *Otolemur* sp.? Evaluating these hypotheses requires data from a region of the face that is relatively removed from the points of application of external forces (i.e., tooth row and areas of muscle attachment) and suitably positioned and shaped to reflect global loading regimes if they exist. The medial orbital wall might be such a place. The medial orbital walls of anthropoids do not have muscles of mastication attaching to them and might therefore be removed from local effects near muscle attachment sites that have been observed in practice (e.g., Hylander and Johnson, 1989) and predicted in theory (Hibbeler, 1997; Chen, 1995). Saint-Venant noted in 1855 that when an external force is applied to a body, there are deformations of the body local to the point of application of the force, but that at a sufficient distance from that point, the stress and strain distribution becomes more uniform. This sufficient distance is generally equal to the largest diameter of the loaded cross section, but in thin-walled members local effects may extend much further into the body (Hibbeler, 1997, p. 120–121). Thus, the medial orbital wall of anthropoids may still be subject to Saint-Venant's effects, but they may be of less importance here than in other parts of the face. In contrast with anthropoids, many strepsirrhines have medial pterygoid muscles attaching to the medial orbital wall within the orbit. This is evidenced in *Otolemur* skulls by a muscle attachment scar on the lower posterior region of the medial orbital wall. It may be that the medial orbital wall of strepsir-

rhines is more strongly affected by Saint-Venant's effects than that of anthropoids, although, as discussed below, this appears not to be the case.

The medial orbital wall is also a good place to evaluate hypotheses regarding loading regimes in the primate face because it is relatively flat, so that it can respond to external loads in a variety of ways. This stands in sharp contrast to the highly curved lateral orbital wall which appears to respond to a variety of external loading regimes predominantly by bending (Ross and Hylander, 1996; Ross and Chen, 1997).

In summary, this paper uses in vivo bone strain data from the medial orbital wall to determine whether: the interorbital region can be modeled as a simple beam under bending or shear; the galago face (and that of anthropoids) is twisting on the brain case during unilateral biting or mastication; the interorbital "pillar" is being axially compressed during incisor loading and both axially compressed and laterally bent during mastication, as predicted by Endo (1966); and the interorbital "pillar" transmits axial compressive forces from the tooth row to the brain case.

## MATERIALS AND METHODS

### Subjects

One adult male owl monkey (*Aotus* sp.?), one adult female greater bushbaby (*Otolemur* sp.?), and four adult female and one subadult male rhesus macaque (*Macaca mulatta*) served as subjects. All of these animals had previously been unilaterally enucleated (i.e., had their orbital contents removed) on the right side for reasons unrelated to this research. This enabled placement of strain gauges on the medial orbital wall and intraorbital roof. In all cases except the male rhesus macaque, enucleation occurred when the animals were adults. In the galago and macaques, no skeletal asymmetries were apparent from measures of orbit diameter based on external landmarks or radiographs. The owl monkey exhibited resorption along the anterior edge of the lateral orbital wall on the enucleated side. Data were only collected from the medial orbital wall and mandible in this animal.

### Strain-gauge placement

During nine separate experiments with the seven individuals, delta (SA-06-030WY-120, Micromeasurements, Raleigh, NC) (wired in a three-wire quarter-bridge circuit) or rectangular rosette strain gauges (FRA 1-11-1L, Texas Measurements, Inc., College Station, TX) (wired in a two-wire quarter bridge circuit) were placed in various combinations on: 1) the medial end of the orbital roof, above the level of the cribriform plate (r, roof; Fig. 3); 2) the medial wall of the bony orbit, on the interorbital septum (uw, upper wall); 3) the os planum of the ethmoid bone as it angles away from the interorbital septum towards the floor of the orbit (lw, lower wall); 4) the anterior root of the zygomatic arch (z, zygoma); and 5) the lateral surface of the mandibular corpus below $M_1$ or $P_4$ (c, corpus; Fig. 5, Table 1). (Additional locations where strain gauge data were recorded by Hylander et al. (1991, 1992, 2000) are also indicated in Fig. 5: di, dorsal interorbital; ri, rostral interorbital.) When placing intraorbital gauges, an attempt was made to orient the gauges so that the B-element was perpendicular to the plane of the orbital aperture. Intraorbital gauge positions are discussed in more detail in Results. Gauge posi-

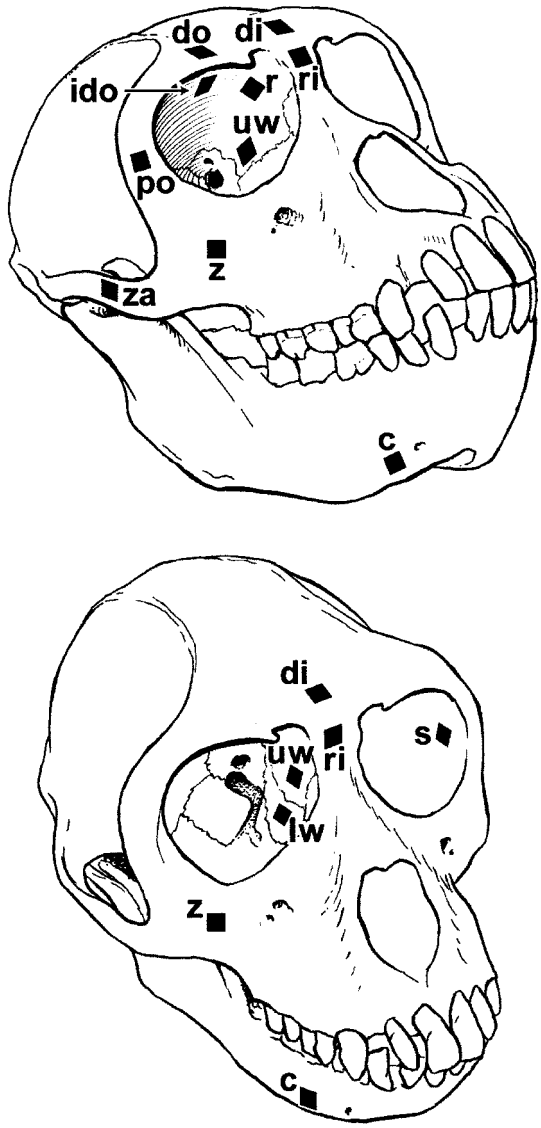


**Fig. 5.** Bony morphology of macaque orbit and strain gauge locations discussed in text. c, corpus, the lateral surface of the mandibular corpus below $M_1$ or $P_4$;di, dorsal interorbital region (Hylander et al., 1991); ri, rostral interorbital region (Hylander et al., 1991); lw, lower wall, the os planum of the ethmoid bone as it angles away from the interorbital septum towards the floor of the orbit; r, roof, the medial end of the orbital roof, above the level of the cribriform plate; uw, upper wall, the medial wall of the bony orbit, on the interorbital septum; z, zygoma, the anterior root of the zygomatic arch. See Table 1 for gauge combinations during each experiment. In this study, data were collected from all positions except di and ri.

*TABLE 1. Experiments from which medial orbital wall data were collected*

| Experiment no. | Individual | Gauge number and type | Gauge locations | Recording frequency (Hz) | Total power strokes |
|---|---|---|---|---|---|
| 5 | *Aotus* 3, male | 2 stacked rectangular rosettes | Right medial orbital wall and right mandibular corpus | 10,000 | 169 |
| 7, no x-ray | *Macaca* 1, female | 3 stacked rectangular rosettes | Right orbital roof, right medial orbital wall, and anterior root of right zygomatic arch | 6,250 | 230 |
| 8 | *Macaca* 2, female | 3 stacked rectangular rosettes | Right orbital roof, right medial orbital wall, and anterior root of right zygomatic arch | 6,250 | 347 |
| 9 | *Macaca* 3, male | 3 stacked rectangular rosettes | Right orbital roof, right medial orbital wall, and anterior root of right zygomatic arch[1] | 6,250 | 212 |
| 28, no x-ray | *Otolemur* sp?, male | 2 stacked delta rosettes | Right medial orbital wall and right mandibular corpus | 600 | 55 |
| 29, no x-ray | *Macaca* 3, male | 2 stacked delta rosettes | Right medial orbital wall and right mandibular corpus | 5400 | 299 |
| 31 | *Aotus* 3, male | 2 stacked delta rosettes | Right medial orbital wall and right mandibular corpus | 2,700 | 337 |
| 41 | *Macaca* 5, female | 2 stacked delta rosettes | Right medial orbital wall and right mandibular corpus[1] | 2,700 | 326 |
| 45 | *Macaca* 4, female | 3 stacked delta rosettes | Upper and lower right medial orbital wall, and right mandibular corpus | 2,700 | 301 |

[1] Data not analyzed because of movement artifact or failed gauge.

tion and orientation were recorded using sketches, notes, and radiographs.

The animals were food-deprived for 24 hr before each experiment, and then one of two anesthesia protocols was followed. In some experiments the animals were heavily sedated using an intramuscular injection of ketamine and acepromazine (Connolly and Quimby, 1978). In others, the animals were anesthetized using inhalant isofluorane. In order to eliminate discomfort to the animal and to abet hemostasis, a local anesthetic (2% lidocaine HCl with epinephrine) was infiltrated subcutaneously over the area where the strain gauge was to be bonded. About 5 min after infiltration, a small incision was made in the skin overlying the gauge site, and the periosteum was elevated to expose the bone. A small area of the cortical bone was degreased with clinical-grade chloroform and neutralized (M-Prep Neutralizer 5A (ammonia water), Measurement Group, Inc., Raleigh, NC), and then the rosette was bonded to it with a cyanoacrylate adhesive. To prevent movements of the lead wires from causing strain in the gauge, the lead wires were bonded to the bone for 3–4 mm, using the same adhesive. Following bonding of the strain gauge and wires, the incision was sutured closed, with the lead wires of the strain gauge passing out through the wound. The lead wires were secured to the skin, using sutures in areas where skin movement is minimal.

## Recording procedure

The owl monkey and galago were placed in a slingsuit (a modified cat-restraint suit) made to specified dimensions by Alice King Medical Arts (Hawthorne, CA). The macaques were placed in a commercially available restraint (XPL-517-CM, Plas Labs, Lansing, MI). These devices restrained the animal's arms while enabling the head and neck to move freely. The animals were allowed to recover for at least 1 hr after isofluorane anesthesia and up to 2 hr after ketamine sedation.

Each of the three elements of the rosettes was connected to form one arm of a Wheatstone bridge. Bridge excitation was 2 volts. Voltage changes were conditioned and amplified on a Vishay 2100 system, and then recorded on a PC at between 0.6–10 kHz (Table 1). Data acquisition to PCs was controlled using LAB-View software (National Instruments, Austin, TX) running in Windows 3.1NT.

The animals were presented hard apricots, hard prunes with pits, gelatin candies ("gummy bears" or "Swedish fish"), nuts (almonds or Brazil nuts), apples, and carrots. Strains were recorded while the animals incised and chewed these foods. The experiments were videotaped, and the subject's behavior (e.g., incision, mastication) and chewing side were recorded on the voice track of the video tape.

After each recording session (or experiment), the animal was again anesthetized and radiographs were taken to document strain gauge position and orientation. The gauges were then removed, the wound was cleaned and closed with sutures, analgesics and antibiotics were administered, and the animal was returned to its cage.

### Strain analysis

At the end of each experiment, data were transferred from the data acquisition PC to a PowerMac or PC for analysis. The data were analyzed in IGOR Pro 3.03 (WaveMetrics, Inc., Lake Oswego, OR), using custom-written software. The strain data were sampled at a rate of 500 Hz and then converted to microstrain, using calibration files made during the recording sessions. Lead wire resistance in the two-wire quarter bridge rectangular rosettes was accounted for by calculating a corrected gauge factor ($K_0$), using the following formula:

$$K_0 = \frac{R}{R + rL} K$$

where K = the gauge factor supplied, R = the nominal resistance of the gauge, r = lead-wire resistance in Ω/m, and L = lead wire length (m).

The strain tracings were examined along with simultaneous electromyograms and the video tapes of the experiments to identify movement artifacts and chewing side. Sequences were selected for analysis on the basis of length, clarity of chewing side, and lack of food manipulation other than incision and mastication. Sometimes early power strokes in a sequence were excluded because the animal was manipulating food, or late power strokes were excluded because the magnitudes of the strains decreased so as to be unreliably distinguishable from noise (which ranged from 5–10 mV in each channel).

Strain ($\epsilon$), a dimensionless unit equaling the change in length of an object divided by its original length, is measured in microstrain ($\mu\epsilon$) units which are equal to $1 \times 10^{-6}$ inches/inch or mm/mm. Tensile strain is registered as a positive value, and compressive strain as a negative value. The maximum principal strain ($\epsilon_1$) is usually the largest tensile strain value, while the minimum principal strain is usually the largest compressive strain value ($\epsilon_2$). $\epsilon_1$ minus $\epsilon_2$ is equal to the maximum shear strain, or $\gamma$-max. For selected sequences, the direction of the maximum principal strain relative to the A-element of the gauge, the magnitude of the shear strains, and the ratio of maximum to minimum strains ($\epsilon_1/|\epsilon_2|$) were calculated according to the equations in Dally and Riley (1965). The magnitude and timing of the peak shear strain were calculated for each power stroke, and then the direction of the maximum principal strain and the ratio of maximum to minimum strains at the same point in time were also calculated. The ratios of shear strain recorded in the medial orbital wall over peak shear strain magnitudes recorded simultaneously elsewhere in the face were also calculated.

### Statistical analyses

Descriptive statistics were calculated for the following variables: magnitude of $\gamma$-max, $\epsilon_1$ orientation, and ratio of $\epsilon_1/|\epsilon_2|$ recorded from the medial orbital wall; $\gamma$-max magnitudes recorded simultaneously from other regions of the face (lateral aspect of the mandibular corpus, orbital roof, and anterior root of the zygoma); and ratio of $\gamma$-max magnitudes in other regions to those recorded from the medial orbital wall. Descriptive statistics were calculated separately for three "bite types:" left chews, right chews, and incisions, both across each experiment and during feeding on different foods. All intraorbital strain gauges were placed in the right orbit, so that all right chews are ipsilateral (working-side) chews, and all left side chews are contralateral (balancing-side) chews.

During experiments 7, 9, 29, and 45, $\gamma$-max exhibited double peaks during a power stroke, and the two peaks were often associated with very different $\epsilon_1$ orientations. Preliminary examination of the data revealed that one group of these peaks always exhibited high values for $\epsilon_1$ orientations (high $\angle$ peaks), and the other always exhibited low values (low $\angle$ peaks) (Fig. 6). Peak data were only gathered on one peak per power stroke: under the assumption that the most important loading regime is the one with the highest strain values, data were gathered from the peak with highest $\gamma$-max value. Descriptive statistics were calculated separately for high $\angle$ and low $\angle$ peaks.

Unpaired two-tailed *t*-tests were used to compare mean $\epsilon_1$ orientations, relative timing of medial orbital wall and corpus strain, and log $\epsilon_1/|\epsilon_2|$ ratios recorded from the same gauge during different "bite types." Unpaired one-sample *t*-tests were used to determine whether mean differences in timing of peak $\gamma$-max in the medial orbital wall and mandibular corpus differed from zero.

**Fig. 6.** Orientation of $\varepsilon_1$ relative to A-element in medial orbital wall plotted against shear strain in the medial orbital wall during experiments 7, 9, 29, and 45. The two clusters of different $\varepsilon_1$ orientations in experiments 7, 9, and 29, and in the lower gauge in experiment 45, correspond to high $\angle$ and low $\angle$ peaks. In experiment 7, high $\angle$ peaks are those in which $\varepsilon_1$ orientation exceeded 70°; low $\angle$ are those in which $\varepsilon_1$ orientation was less than 30°. In experiment 9, there is no clear division between high $\angle$ and low $\angle$ peaks, so a relatively arbitrary division was made. Low $\angle$ were designated as those in which $\varepsilon_1$ orientation was less than 125°; high $\angle$ peaks were designated as those in which $\varepsilon_1$ orientation exceeded 125°. In experiment 29, high $\angle$ peaks are those in which $\varepsilon_1$ orientation exceeded 120°; low $\angle$ are those in which $\varepsilon_1$ orientation was less than 90°. In experiment 45, high $\angle$ peaks are those in which $\varepsilon_1$ orientation exceeded 80°; low $\angle$ are those in which $\varepsilon_1$ orientation was less than 60°.

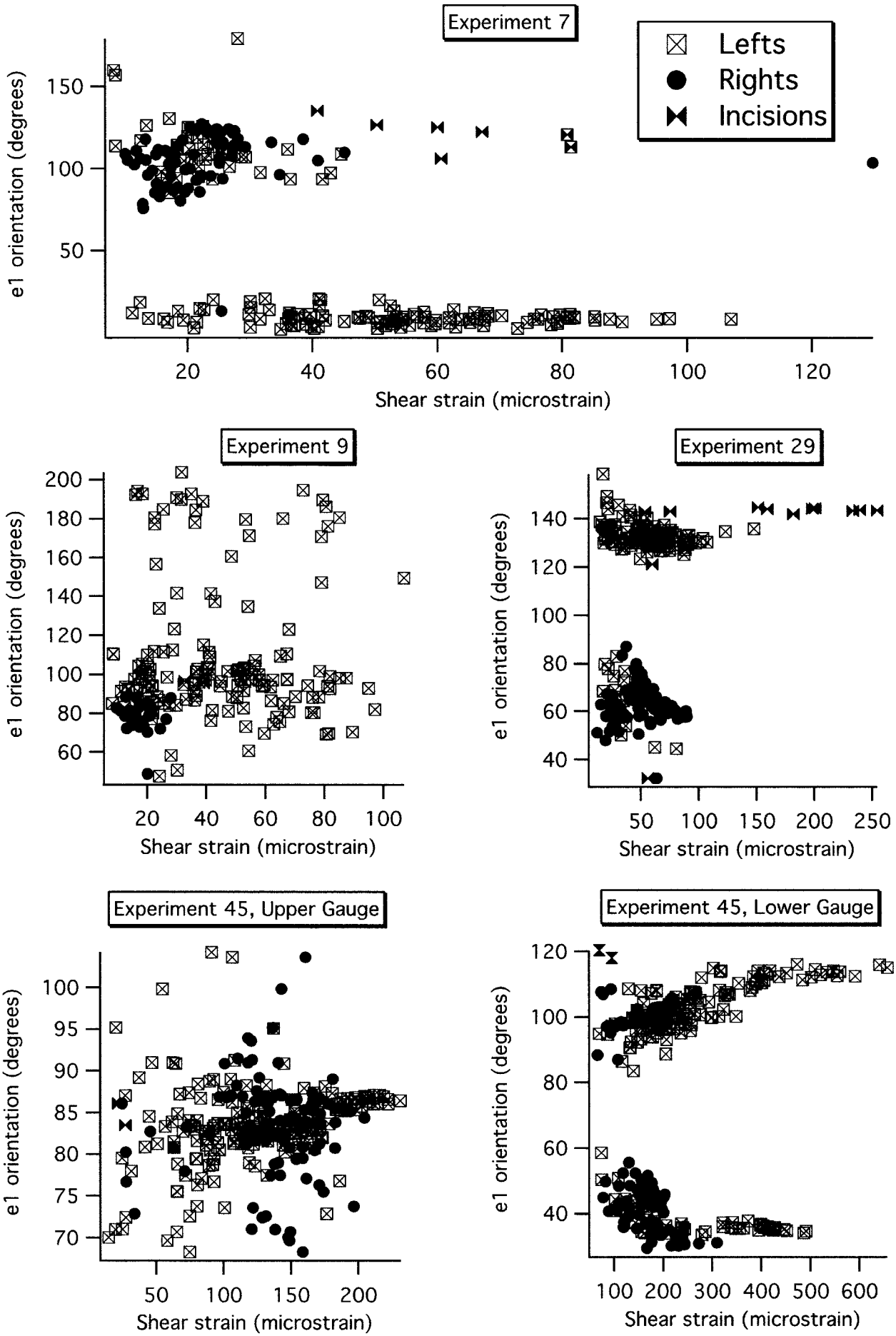
Experiment 7
Lefts
Rights
Incisions
e1 orientation (degrees)
Shear strain (microstrain)
Experiment 9
Experiment 29
Experiment 45, Upper Gauge
Experiment 45, Lower Gauge

Fig. 6.

*TABLE 2. Descriptive statistics for experiment 5: rosettes on right medial orbital wall (wall) and right mandibular corpus (corpus) of* Aotus *3 (male)*

| | | γ-max (με) | | | Ratio $\varepsilon_1/\lvert\varepsilon_2\rvert$ | | $\varepsilon_1$ orientation[1] | |
|---|---|---|---|---|---|---|---|---|
| Food, gauge, side | N | Mean | SD | Max | Mean | SD | Mean | SD |
| All foods | | | | | | | | |
| Wall | | | | | | | | |
| Left | 135 | 148 | 97.3 | 418.0 | 0.82 | 0.305 | 47.0 | 20.1 |
| Right | 34 | 160 | 84.4 | 396.0 | 0.79 | 0.400 | 65.0 | 41.6 |
| | | | | | Ratio corpus γ-max/wall γ-max | | | |
| | | | | | Mean | SD | Max | Min |
| Corpus | | | | | | | | |
| Left | 135 | 961 | 346.2 | 2,084 | 11.5 | 11.22 | 52.0 | 1.2 |
| Right | 34 | 1,069 | 217.0 | 1,736 | 8.7 | 4.89 | 20.6 | 2.9 |
| Apricot and peach | | | | | | | | |
| Wall | | | | | | | | |
| Left | 63 | 81 | 46.4 | 192.4 | 0.90 | 0.213 | 40.0 | 17.2 |
| Right | 28 | 180 | 78.5 | 395.8 | 0.66 | 0.223 | 49.0 | 16.3 |
| | | | | | Ratio corpus γ-max/wall γ-max | | | |
| | | | | | Mean | SD | Max | Min |
| Corpus | | | | | | | | |
| Left | 63 | 854 | 224.8 | 1,320.0 | 16.3 | 13.14 | 52.0 | 4.64 |
| Right | 28 | 1,090 | 231.6 | 1,737.0 | 7.2 | 3.96 | 20.6 | 2.9 |
| Prune | | | | | | | | |
| Wall | | | | | | | | |
| Left | 72 | 206 | 92.4 | 418.0 | 0.75 | 0.355 | 53.0 | 20.7 |
| Right | 6 | 63 | 4.4 | 67.0 | 1.4 | 0.522 | 142.0 | 36.7 |
| | | | | | Ratio corpus γ-max/wall γ-max | | | |
| | | | | | Mean | SD | Max | Min |
| Corpus | | | | | | | | |
| Left | 72 | 1,056 | 403.5 | 2,084.0 | 7.3 | 6.96 | 41.7 | 1.2 |
| Right | 6 | 969 | 80.5 | 1,032.0 | 15.5 | 2.20 | 18.0 | 12.6 |

[1] Relative to A-element. Max, maximum; Min, minimum.

## RESULTS

### Bony morphology

The intraorbital surface of the bony orbit of *Macaca mulatta* is roughly cone-shaped, with the apex of the cone lying in the region of the optic canal and the base forming the orbital aperture (Fig. 5). The roof of the orbit is formed by the orbital plate of the frontal bone, which also forms the floor of the anterior cranial fossa and the inferior aspect of the supraorbital torus. Medially, the frontal bone curves inferiorly to form simultaneously the upper portion of the medial orbital wall and the lateral wall of the olfactory pit of the anterior cranial fossa. The morphology of the medial orbital wall varies below the level of the anterior cranial base (planum sphenoideum posteriorly and cribriform plate anteriorly). Below the planum sphenoideum and anteromedial to the openings of the optic canals, the frontal bones of each side fuse with each other to form the thin interorbital septum (upper wall, Fig. 5). Below the cribriform plate, there is no interorbital septum because the os planum of the ethmoid slants inferolaterally towards the floor of the orbit, simultaneously forming the lower part of the medial orbital wall and the lateral wall of the nasal cavity or paranasal sinus. The medial orbital wall receives minor contributions from the lacrimal and maxilla anteriorly and the lesser wing of sphenoid and palatine posteriorly. Gauges were placed in three locations within the orbit. The majority of medial orbital wall strains were recorded from the portion of the frontal bone making up the interorbital septum. In experiment 45, strains were recorded from the os planum of the ethmoid in the lower orbital wall (lw), and in two experiments strains were successfully recorded from the frontal bone on the medial aspect of the orbital roof (Fig. 5).

### Data collection problems

Not all animals would eat all the kinds of food presented to them during each experiment. For example, *Macaca* 1 only ate apples during experiment 7, *Macaca* 3 only ate almonds and dates during experiment 9, and *Otolemur* only ate gelatin candies during experiment 28. The animals often showed a preference for chewing on one side during an experiment, and usually the left side (Tables 2–10). All mandibular corpus gauges were placed on the right side and all animals had been enucleated on the right side, so the animals may have either minimized chewing ipsilateral to the corpus gauge or to the enucleated orbit. Two gauges exhibited movement artifacts and/or failed completely at some time during the experiment (Table 1). Radiographs taken

*TABLE 3. Descriptive statistics for experiment 7: rosettes on right orbital roof (roof), medial orbital wall (wall), and anterior root of zygomatic arch (arch) of* Macaca *1 (female)*

| Food, gauge, side | N | γ-max (με) | | | Ratio $\varepsilon_1/\lvert\varepsilon_2\rvert$ | | $\varepsilon_1$ orientation[1] | |
|---|---|---|---|---|---|---|---|---|
| | | Mean | SD | Max | Mean | SD | Mean | SD |
| Apple | | | | | | | | |
| Wall | | | | | | | | |
| Incision | 7 | 63 | 15.0 | 81 | 1.2 | 0.16 | 121.0 | 9.5 |
| Left (high ∠)[2] | 41 | 23 | 8.5 | 107 | 14.3 | 27.13 | 112.0 | 18.5 |
| Left (low ∠)[2] | 107 | 53 | 20.8 | 107 | 2.2 | 7.13 | 9.0 | 4.2 |
| Right (high ∠)[2] | 68 | 23 | 15.0 | 130 | 3.1 | 4.63 | 105.0 | 13.4 |
| Right (low ∠)[2] | 2 | 31 | 7.5 | 36 | 2.6 | 0.66 | 12.0 | 1.6 |
| | | | | | Ratio roof γ-max/wall γ-max | | | |
| | | | | | Mean | SD | Max | Min |
| Roof | | | | | | | | |
| Incision | 7 | 44 | 16.4 | 63 | 0.7 | 0.17 | 0.83 | 0.3 |
| Left | 153 | 46 | 19.8 | 99 | 1.2 | 0.64 | 4.3 | 0.5 |
| Right | 70 | 17 | 14.6 | 106 | 0.7 | 0.29 | 2.0 | 0.1 |
| | | | | | Ratio arch γ-max/wall γ-max | | | |
| | | | | | Mean | SD | Max | Min |
| Arch | | | | | | | | |
| Incision | 7 | 182 | 104.8 | 386 | 2.8 | 1.11 | 4.8 | 1.7 |
| Left | 153 | 192 | 79.9 | 555 | 5.4 | 3.70 | 19.4 | 1.3 |
| Right | 70 | 180 | 64.2 | 336 | 8.8 | 3.06 | 15.9 | 1.1 |

[1] Relative to A-element. Max, maximum; Min, minimum.
[2] High ∠, power strokes in which $\varepsilon_1$ orientation exceeded 70°; low ∠, power strokes in which $\varepsilon_1$ orientation was less than 30°. No power strokes fell between these values.

during experiments 7, 28, and 29 were not adequately exposed, so gauge position and orientation in these experiments are estimated from sketches and notes made during surgeries.

### Bone strain orientations

The mean orientations of $\epsilon_1$ (maximum principal (tensile) strain) during incision, right, and left chews during each experiment are illustrated in Figures 7–10. Descriptive statistics for these data are given in Tables 2–10. The $\epsilon_1$ orientations are illustrated on tracings from the lateral radiographs taken after gauge placement. In the case of experiments 7, 28, and 29, for which radiographs are not available, $\epsilon_1$ orientations are illustrated on sketches of skulls, with the orientation of the A-element derived from sketches and notes taken after gauge placement (Figs. 8, 10). The notes suggest that in these three cases, the gauges were placed so that the middle element of the rosette was aligned roughly perpendicular to the plane of the orbital aperture, and this is how the data are presented. The strain orientations resulting from applying this assumption to experiments 7 and 29 are similar to those recorded during other experiments, although rotated slightly counterclockwise (Fig. 10).

***Incision.*** No incision data are available for experiment 5 on *Aotus*, from experiment 28 on *Otolemur*, or experiment 41 on *Macaca*. *Otolemur* has a toothcomb and small upper incisors which it does not use for powerful incisor biting, at least not in a laboratory setting. In the other cases, the animals would not perform powerful incision of food or the data were not suitable for analysis. In the majority of experiments, mean $\epsilon_1$ orientation during incision is oriented anterosuperiorly but is more vertically oriented relative to the tooth row than $\epsilon_1$ orientation during mastication (Figs. 7, 10). Mean $\epsilon_1$ orientation during incision in experiment 29 is almost vertical relative to the tooth row (Fig. 10). In experiment 9, mean $\epsilon_1$ during incision is intermediate between that during right and left chews (Fig. 9). Mean $\epsilon_1$ orientations during incision are significantly different from those recorded during mastication in 4 out of 6 experiments for which incision data are available. In experiment 9, mean incision $\epsilon_1$ orientation is not significantly different from mean left chew orientation (Fig. 8), and in experiment 45, mean incision $\epsilon_1$ orientation in the upper gauge is not significantly different from either mean left or mean right orientations (Fig. 8).

***Mastication.*** During experiments 7, 9, 29 (medial orbital wall gauge), and 45 (lower medial orbital wall gauge) (all on *Macaca*), γ-max exhibited double peaks during some mastication power strokes. Data were only gathered on one peak per power stroke and always from the peak with highest γ-max value. Because $\epsilon_1$ orientations differed between these two peaks (Fig. 6), mean $\epsilon_1$ orientations for the high ∠ peaks are separated from those for the low ∠ peaks. The $\epsilon_1$ orientations of the high ∠ peaks in experiments 7, 9, 29, and 45 closely resemble the $\epsilon_1$ orientations recorded during the single peaks of the other experiments, so these data are arbitrarily presented and discussed together first (Figs. 9, 10). The low ∠ peaks are then discussed separately.

*TABLE 4. Descriptive statistics for experiment 8: rosettes on right orbital roof (roof), medial orbital wall (wall), and anterior root of zygomatic arch (arch) of* Macaca *2 (female)*

| | | μ-max (με) | | | Ratio $\varepsilon_1/\lvert\varepsilon_2\rvert$ | | $\varepsilon_1$ orientation[1] | |
|---|---|---|---|---|---|---|---|---|
| Food, gauge, side | N | Mean | SD | Max | Mean | SD | Mean | SD |
| All foods | | | | | | | | |
| Wall | | | | | | | | |
| Incision | 36 | 95 | 37.8 | 202 | 0.9 | 0.10 | 126.0 | 11.0 |
| Left | 142 | 66 | 31.3 | 221 | 1.7 | 0.60 | 85.0 | 19.3 |
| Right | 156 | 58 | 25.3 | 132 | 1.5 | 0.52 | 89.0 | 18.6 |
| | | | | | Ratio roof γ-max/wall γ-max | | | |
| | | | | | Mean | SD | Max | Min |
| Roof | | | | | | | | |
| Incision | 36 | 54 | 25.4 | 140 | 0.7 | 0.52 | 2.4 | 0.2 |
| Left | 140 | 26 | 18.6 | 104 | 0.4 | 0.31 | 2.6 | 0.1 |
| Right | 118 | 19 | 10.1 | 55 | 0.3 | 0.14 | 0.9 | 0.1 |
| | | | | | Ratio arch γ-max/wall γ-max | | | |
| | | | | | Mean | SD | Max | Min |
| Arch | | | | | | | | |
| Incision | 36 | 332 | 314.9 | 1441 | 3.4 | 2.66 | 13.4 | 1.5 |
| Left | 142 | 1,099 | 167.6 | 1834 | 19.7 | 8.1 | 47.6 | 7.4 |
| Right | 169 | 914 | 203.2 | 1296 | 19.0 | 9.5 | 61.3 | 3.7 |
| Date | | | | | | | | |
| Wall | | | | | | | | |
| Incision | 36 | 100 | 25.9 | 137 | 1.0 | 0.06 | 112.0 | 20.5 |
| Left | 142 | 99 | 34.1 | 221 | 1.7 | 0.20 | 80.0 | 9.8 |
| Right | 156 | 73 | 25.2 | 132 | 1.5 | 0.33 | 88.0 | 17.2 |
| | | | | | Ratio roof γ-max/wall γ-max | | | |
| | | | | | Mean | SD | Max | Min |
| Roof | | | | | | | | |
| Incision | 36 | 42 | 14.1 | 65 | 0.44 | 0.19 | 0.7 | 0.2 |
| Left | 140 | 33 | 14.2 | 82 | 0.33 | 0.08 | 0.6 | 0.2 |
| Right | 118 | 23 | 11.3 | 55 | 0.33 | 0.13 | 0.7 | 0.1 |
| | | | | | Ratio arch γ-max/wall γ-max | | | |
| | | | | | Mean | SD | Max | Min |
| Arch | | | | | | | | |
| Incision | 36 | 810 | 547.1 | 1,441 | 7.7 | 4.4 | 13.4 | 3.5 |
| Left | 142 | 1,218 | 196.6 | 1,834 | 13.5 | 5.2 | 38.1 | 8.3 |
| Right | 169 | 874 | 215.8 | 1,296 | 13.0 | 4.5 | 29.2 | 4.9 |
| Almond | | | | | | | | |
| Wall | | | | | | | | |
| Incision | 6 | 152 | 31.7 | 202 | 0.9 | 0.08 | 128.0 | 0.91 |
| Left | 86 | 51 | 16.2 | 104 | 1.7 | 0.73 | 89.0 | 20.8 |
| Right | 36 | 49 | 15.4 | 81 | 1.9 | 0.78 | 88.0 | 16.1 |
| | | | | | Ratio roof γ-max/wall γ-max | | | |
| | | | | | Mean | SD | Max | Min |
| Roof | | | | | | | | |
| Incision | 6 | 82 | 12.5 | 100 | 0.5 | 0.05 | 0.6 | 0.5 |
| Left | 84 | 16 | 6.0 | 36 | 0.3 | 0.11 | 0.7 | 0.1 |
| Right | 35 | 16 | 6.1 | 32 | 0.3 | 0.08 | 0.5 | 0.2 |
| | | | | | Ratio arch γ-max/wall γ-max | | | |
| | | | | | Mean | SD | Max | Min |
| Arch | | | | | | | | |
| Incision | 6 | 354 | 68.5 | 467 | 2.3 | 0.28 | 2.6 | 1.9 |
| Left | 86 | 1,078 | 98.3 | 1,213 | 23.4 | 7.64 | 47.6 | 11.2 |
| Right | 36 | 1,040 | 142.7 | 1,248 | 23.2 | 7.48 | 44.9 | 10.6 |
| Gelatin candy | | | | | | | | |
| Wall | | | | | | | | |
| Incision | 4 | 47 | 13.6 | 59 | 0.9 | 0.13 | 127.0 | 3.2 |
| Left | 16 | 64 | 19.8 | 106 | 1.7 | 0.51 | 72.0 | 21.5 |

*(continued)*

*TABLE 4. (Continued)*

| Food, gauge, side | N | γ-max (με) | | | Ratio $\varepsilon_1/\lvert\varepsilon_2\rvert$ | | $\varepsilon_1$ orientation[1] | |
|---|---|---|---|---|---|---|---|---|
| | | Mean | SD | Max | Mean | SD | Mean | SD |
| | | | | | Ratio roof γ-max/wall γ-max | | | |
| | | | | | Mean | SD | Max | Min |
| Roof | | | | | | | | |
| Incision | 4 | 94 | 33.4 | 140 | 2.0 | 0.46 | 2.4 | 1.4 |
| Left | 16 | 63 | 16.7 | 104 | 1.1 | 0.50 | 2.6 | 0.7 |
| | | | | | Ratio arch γ-max/wall γ-max | | | |
| | | | | | Mean | SD | Max | Min |
| Arch | | | | | | | | |
| Incision | 4 | 194 | 94.7 | 287 | 3.9 | 1.03 | 4.9 | 2.5 |
| Left | 16 | 917 | 182.9 | 1,113 | 15.2 | 4.42 | 23.5 | 7.4 |
| Carrot | | | | | | | | |
| Wall | | | | | | | | |
| Right | 26 | 31 | 8.5 | 52 | 1.3 | 0.34 | 84.0 | 17.4 |
| | | | | | Ratio roof γ-max/wall γ-max | | | |
| | | | | | Mean | SD | Max | Min |
| Roof | | | | | | | | |
| Right | 28 | 12 | 6.6 | 39 | 0.4 | 0.17 | 0.8 | 0.2 |
| | | | | | Ratio arch γ-max/wall γ-max | | | |
| | | | | | Mean | SD | Max | Min |
| Arch | | | | | | | | |
| Right | 39 | 886 | 130.1 | 1,090 | 30.0 | 7.3 | 53.3 | 18.9 |

[1] Relative to A-element. Max, maximum; Min, minimum.

***High ∠ peaks.*** As noted above, all intraorbital strain gauges were placed in the right orbit, so during all right chews the intraorbital gauges are on the working side, and during all left chews, the intraorbital gauges are on the balancing side. In all except experiment 28 on the *Otolemur*, and experiment 41 on a *Macaca*, mean $\epsilon_1$ orientations during mastication are anterosuperior (Figs. 9, 10). Mean $\epsilon_1$ orientations recorded during mastication in experiment 41 are anteroinferior (Fig. 8). Mean left-chew $\epsilon_1$ orientations are significantly different from mean right-chew orientations (not separated by food type) in 7 out of 9 experiments. In experiment 5, mean $\epsilon_1$ orientations during right chews are oriented counterclockwise of those recorded during left chews; in the remaining six experiments, mean $\epsilon_1$ orientations during right chews are oriented clockwise of those recorded during left chews. Mean $\epsilon_1$ orientations recorded from *Otolemur* during mastication in experiment 28 are anterosuperior during right chews and anteroinferior during left chews. In experiments 8 and 41, mean left- and mean right-chew $\epsilon_1$ orientations are not significantly different, at $P < 0.05$.

***Low ∠ peaks.*** In Figure 11, mean $\epsilon_1$ orientations representing low ∠ peaks are shown for experiments 7, 9, 29 (medial orbital wall gauge), and 45 (lower medial orbital wall gauge). The mean differences between the high ∠ and low ∠ values of $\epsilon_1$ orientation are: experiment 7, 100°; experiment 9, 79°; experiment 29, 70°; and experiment 45 (lower gauge), 63°. All are significantly different, at $P < 0.0001$. In experiments 7 and 9, $\epsilon_1$ orientation of the low ∠ peaks is anteroinferior (Fig. 11), resembling the single peaks recorded during experiment 41 (Fig. 9). In experiments 29 and 45 (lower gauge; Figs. 9, 10), $\epsilon_1$ orientation is primarily anterior, although slightly superior in experiment 29 and slightly inferior during experiment 45 (Fig. 11). In experiments 9, 29 (medial orbital wall gauge), and 45 (lower medial orbital wall gauge), the high ∠ peaks were predominantly found on the balancing side medial orbital wall (i.e., were associated with left chews), and the low ∠ peaks were predominantly found on the working side. In experiment 7 the reverse was true.

## Bone strain magnitudes

Descriptive statistics for shear strain magnitudes recorded from the medial orbital wall, the orbital roof, the anterior root of the zygomatic arch and the lateral aspect of the mandibular corpus during incision and mastication of various foods are given in Tables 2–10. The ratios of strains from other areas in the face to those recorded from the medial orbital wall are also given.

Mean γ-max values recorded during the three different power-stroke types (incision, working-, and balancing-side chews) range from 148–319 με in *Aotus* (Tables 2 and 8), from 18–263 με in *Macaca* (Tables 3–5, 7, 9, and 10), and from 143–346 με in *Otolemur* (Table 6). *Otolemur* and *Aotus* exhibit higher mean γ-max than *Macaca*. The highest mean strains recorded during mastication of any food were elicited by dried papaya (only the owl monkey ate dried papaya) (Table 8). Similar strain magnitudes

*TABLE 5. Descriptive statistics for experiment 9: rosettes on right medial orbital wall (wall) and right anterior root of zygomatic arch (arch) of* Macaca *3*

| | | γ-max (με) | | | Ratio $\varepsilon_1/\lvert\varepsilon_2\rvert$ | | $\varepsilon_1$ orientation[1] | |
|---|---|---|---|---|---|---|---|---|
| Food, gauge, side | N | Mean | SD | Max | Mean | SD | Mean | SD |
| All foods | | | | | | | | |
| Wall | | | | | | | | |
| Incision | 2 | 36 | 4.5 | 39 | 0.0 | 0.36 | 96.0 | 0.9 |
| Left (low ∠)[2] | 135 | 30 | 10.5 | 54 | 0.3 | 0.31 | 93.0 | 13.0 |
| Left (high ∠)[2] | 44 | 28 | 10.9 | 58 | 3.2 | 10.24 | 170.0 | 20.1 |
| Right | 31 | 18 | 4.2 | 28 | 0.0 | 0.09 | 79.0 | 7.5 |
| | | | | | Ratio arch γ-max/wall γ-max | | | |
| | | | | | Mean | SD | Max | Min |
| Arch | | | | | | | | |
| Incision | 2 | 260 | 267.5 | 449 | 7.6 | 8.43 | 13.7 | 1.8 |
| Left | 179 | 312 | 106.7 | 723 | 11.9 | 5.51 | 32.6 | 1.8 |
| Right | 31 | 252 | 68.4 | 392 | 14.3 | 3.67 | 23.8 | 7.8 |
| Almond | | | | | | | | |
| Wall | | | | | | | | |
| Left (low ∠)[2] | 42 | 25 | 8.2 | 42 | 0.2 | 0.10 | 83.0 | 10.6 |
| Left (high ∠)[2] | 14 | 22 | 6.7 | 35 | 3.1 | 4.71 | 183.0 | 10.5 |
| Right | 31 | 18 | 4.2 | 28 | 0.1 | 0.05 | 79.0 | 7.5 |
| | | | | | Ratio arch γ-max/wall γ-max | | | |
| | | | | | Mean | SD | Max | Min |
| Arch | | | | | | | | |
| Left | 56 | 321 | 70.0 | 447 | 14.5 | 5.32 | 32.6 | 7.3 |
| Right | 31 | 252 | 68.4 | 392 | 14.3 | 3.67 | 23.8 | 7.8 |
| Date | | | | | | | | |
| Wall | | | | | | | | |
| Left (low ∠)[2] | 93 | 33 | 10.6 | 54 | 0.4 | 0.35 | 98.0 | 11.1 |
| Left (high ∠)[2] | 30 | 30 | 11.5 | 58 | 3.3 | 12.06 | 163.0 | 20.6 |
| | | | | | Ratio corpus γ-max/wall γ-max | | | |
| | | | | | Mean | SD | Max | Min |
| Arch | | | | | | | | |
| Left | 123 | 307 | 120.0 | 723 | 10.7 | 5.19 | 30.9 | 1.8 |

[1] Relative to A-element. Max, maximum; Min, minimum.
[2] Low ∠, power strokes in which $\varepsilon_1$ orientation was less than 125°; high ∠, power strokes in which $\varepsilon_1$ orientation exceeded 125°. This division was relatively arbitrary.

*TABLE 6. Descriptive statistics for experiment 28: rosettes on right medial orbital wall (wall), and right mandibular corpus (corpus) of* Otolemur *sp*

| | | γ-max (με) | | | Ratio $\varepsilon_1/\lvert\varepsilon_2\rvert$ | | $\varepsilon_1$ orientation[1] | |
|---|---|---|---|---|---|---|---|---|
| Food, gauge, side | N | Mean | SD | Max | Mean | SD | Mean | SD |
| Gelatin candy | | | | | | | | |
| Wall | | | | | | | | |
| Left | 20 | 143 | 60.2 | 266 | 2.2 | 0.63 | 136.0 | 13.1 |
| Right | 35 | 346 | 146.4 | 609 | 0.3 | 0.70 | 59.0 | 9.6 |
| | | | | | Ratio corpus γ-max/wall γ-max | | | |
| | | | | | Mean | SD | Max | Min |
| Corpus | | | | | | | | |
| Left | 20 | 486 | 336.0 | 1,239 | 3.1 | 1.28 | 5.4 | 1.3 |
| Right | 35 | 1841 | 674.6 | 2,708 | 5.5 | 1.61 | 8.9 | 2.5 |

[1] Relative to A-element. Max, maximum; Min, minimum.

were recorded during mastication of gelatin candies. The next highest mean shear strain magnitudes were elicited by dried prune. The maximum strains in the medial orbital wall of the macaques (657 με) were recorded during a contralateral chew of dried prune (Table 10). The maximum strains recorded from the medial orbital wall of the galago (609 με) (Table 6) and the owl monkey (1,294 με) (Table 7) were recorded during an ipsilateral chew of gelatin candy. The maximum γ-max values recorded from the medial orbital wall during each experiment are 418 and 1,294 in the two experiments on *Aotus* (Tables 2 and 8), range from 58–657 με in the *Macaca* experiments (Tables 3–5, 7, 9, and 10), and are 609 με in the *Otolemur* experiment (Table 6).

*TABLE 7. Descriptive statistics for experiment 29: rosettes on right medial orbital wall (wall) and right mandibular corpus (corpus) of* Macaca *3*

| Food, gauge, side | N | γ-max (με) | | | Ratio $\varepsilon_1/\lvert\varepsilon_2\rvert$ | | $\varepsilon_1$ orientation[1] | |
|---|---|---|---|---|---|---|---|---|
| | | Mean | SD | Max | Mean | SD | Mean | SD |
| All foods | | | | | | | | |
| Wall | | | | | | | | |
| Incision | 13 | 150 | 74.5 | 254 | 1.8 | 0.52 | 135.0 | 20.7 |
| Left (high ∠)[2] | 111 | 53 | 24.7 | 148 | 10.0 | 65.7 | 133.0 | 5.1 |
| Left (low ∠)[2] | 21 | 37 | 16.1 | 81 | 1.0 | 8.3 | 65.0 | 10.7 |
| Right (high ∠)[2] | 2 | 21 | 6.1 | 25 | 0.1 | 0.10 | 137.0 | 1.3 |
| Right (low ∠)[2] | 141 | 51 | 16.2 | 90 | 0.8 | 7.7 | 64.0 | 7.3 |
| | | | | | Ratio corpus γ-max/wall γ-max | | | |
| | | | | | Mean | SD | Max | Min |
| Corpus | | | | | | | | |
| Incision | 14 | 652 | 212.6 | 941 | 5.2 | 2.50 | 11.6 | 3.0 |
| Left | 133 | 370 | 141.4 | 714 | 7.8 | 4.52 | 46.9 | 3.9 |
| Right | 152 | 449 | 103.4 | 635 | 9.4 | 2.67 | 23.9 | 3.8 |
| Almond | | | | | | | | |
| Wall | | | | | | | | |
| Incision | 2 | 59 | 1.4 | 60 | 1.8 | 1.44 | 125.0 | 6.0 |
| Left (high ∠)[2] | 107 | 57 | 25.1 | 148 | 10.0 | 0.2 | 133.0 | 5.1 |
| Left (low ∠)[2] | 5 | 34 | 17.3 | 62 | 5.5 | 17.6 | 62.0 | 11.9 |
| Right (high ∠)[2] | 2 | 21 | 6.1 | 25 | 0.1 | 0.10 | 137.0 | 1.3 |
| Right (low ∠)[2] | 141 | 51 | 16.2 | 90 | 0.8 | 7.7 | 65.0 | 9.0 |
| | | | | | Ratio corpus γ-max/wall γ-max | | | |
| | | | | | Mean | SD | Max | Min |
| Corpus | | | | | | | | |
| Incision | 3 | 556 | 108.8 | 682 | 9.5 | 1.80 | 11.6 | 8.3 |
| Left | 113 | 396 | 137.8 | 714 | 8.1 | 4.81 | 46.9 | 3.9 |
| Right | 152 | 449 | 103.4 | 635 | 9.4 | 2.67 | 23.9 | 3.8 |
| Gelatin candy | | | | | | | | |
| Wall | | | | | | | | |
| Incision | 11 | 175 | 63.7 | 254 | 1.6 | 0.40 | 143.0 | 1.3 |
| Left (high ∠)[2] | 4 | 46 | 9.3 | 55 | 10.0 | 6.30 | 129.0 | 4.3 |
| Left (low ∠)[2] | 16 | 39 | 16.1 | 81 | 0.4 | 0.14 | 67.0 | 10.4 |
| | | | | | Ratio corpus γ-max/wall γ-max | | | |
| | | | | | Mean | SD | Max | Min |
| Corpus | | | | | | | | |
| Incision | 11 | 678 | 230.0 | 941 | 4.0 | 0.70 | 4.9 | 3.0 |
| Left | 20 | 227 | 39.8 | 316 | 6.1 | 1.46 | 8.4 | 3.9 |

[1] Relative to A-element. Max, maximum; Min, minimum.
[2] High ∠, power strokes in which $\varepsilon_1$ orientation exceeded 120°; low ∠, power strokes in which $\varepsilon_1$ orientation was less than 90°. No power strokes fell between these values.

Relative to the mandibular corpus, strain magnitudes recorded from the medial orbital wall are low. In the owl monkey, the mandibular corpus strains are usually more than twice those recorded simultaneously from the medial orbital wall (Table 8), and often averaged 15–16 times higher (Table 2). In the galago, corpus strains were always higher than the medial orbital wall strains, averaging 3–5 times higher (Table 6). In macaques, the mandibular corpus strains were also much higher than those recorded from the medial orbital wall, averaging from 4–9.5 times as high in experiment 29 (Tables 4, 5, 7, 9, and 10). In experiment 45, in which gauges were placed on the upper and lower medial orbital wall, the upper gauge showed consistently low shear strain magnitudes in comparison with the mandibular corpus (Table 9). Occasionally the lower gauge on the medial orbital wall would register higher shear strains than the mandibular corpus, but only during mastication contralateral to the two gauges (i.e., on the left side), and only at very low strain magnitudes.

In the three macaque experiments (7–9) in which strains were recorded simultaneously from the both the medial orbital wall and the anterior root of the zygomatic arch, strains from the medial orbital wall were always lower than those recorded from the zygoma (Tables 3–5). Strains in the zygoma ranged from 1.1 times as high to 48 times as high as those recorded from the medial orbital wall. In experiments 8 and 9, medial orbital wall strains relative to the zygoma strains were higher during incisions than during mastication (Tables 4 and 5). The opposite was true during experiment 7 (Table 3).

In experiments 7 and 8, strains were also simultaneously recorded from the medial end of the roof of the orbit, adjacent to the midline cranial base (Tables 3 and 4). In experiment 7, the average strains

*TABLE 8. Descriptive statistics for experiment 31: rosettes on right medial orbital wall (wall), and right mandibular corpus (corpus) of* Aotus *3*

| Food, gauge, side | N | γ-max (με) Mean | γ-max (με) SD | γ-max (με) Max | Ratio $\varepsilon_1/\lvert\varepsilon_2\rvert$ Mean | Ratio $\varepsilon_1/\lvert\varepsilon_2\rvert$ SD | $\varepsilon_1$ orientation[1] Mean | $\varepsilon_1$ orientation[1] SD |
|---|---|---|---|---|---|---|---|---|
| All foods | | | | | | | | |
| Wall | | | | | | | | |
| Incision | 41 | 188 | 114.6 | 658 | 1.0 | 0.37 | 112 | 12.1 |
| Left | 111 | 222 | 91.5 | 454 | 1.8 | 0.95 | 91 | 18.7 |
| Right | 185 | 319 | 192.6 | 1,294 | 0.5 | 0.35 | 52 | 13.2 |

| | | Ratio corpus γ-max/wall γ-max Mean | SD | Max | Min |
|---|---|---|---|---|---|
| Corpus | | | | | |
| Incision | 41 | 6.0 | 1.31 | 9.1 | 1.7 |
| Left | 111 | 3.7 | 1.58 | 9.8 | 1.4 |
| Right | 185 | 2.5 | 1.3 | 8.6 | 0.8 |
| Prune | | | | | |
| Wall | | | | | |
| Incision | 5 | 1.1 | 0.43 | 111 | 8.1 |
| Left | 15 | 1.9 | 0.58 | 104 | 8.6 |
| Right | 65 | 0.6 | 0.48 | 54 | 11.8 |

| | | Ratio corpus γ-max/wall γ-max Mean | SD | Max | Min |
|---|---|---|---|---|---|
| Corpus | | | | | |
| Incision | 5 | 5.0 | 0.61 | 5.6 | 4.2 |
| Left | 15 | 4.1 | 1.30 | 7.3 | 3.3 |
| Right | 65 | 2.4 | 1.04 | 6.4 | 1.0 |
| Gelatin candy | | | | | |
| Wall | | | | | |
| Incision | 24 | 0.9 | 0.40 | 111 | 14.9 |
| Left | 12 | 2.0 | 0.30 | 93 | 10.0 |
| Right | 42 | 0.4 | 0.25 | 57 | 12.9 |

| | | Ratio corpus γ-max/wall γ-max Mean | SD | Max | Min |
|---|---|---|---|---|---|
| Corpus | | | | | |
| Incision | 24 | 6.1 | 1.44 | 9.1 | 1.7 |
| Left | 12 | 3.5 | 0.54 | 4.6 | 2.6 |
| Right | 42 | 3.4 | 1.49 | 8.6 | 1.0 |
| Papaya | | | | | |
| Wall | | | | | |
| Incision | 3 | 0.9 | 0.25 | 112 | 6.7 |
| Left | 21 | 2.0 | 0.30 | 85 | 23.8 |
| Right | 17 | 0.4 | 0.25 | 48 | 6.1 |

| | | Ratio corpus γ-max/wall γ-max Mean | SD | Max | Min |
|---|---|---|---|---|---|
| Corpus | | | | | |
| Incision | 3 | 6.9 | 1.74 | 8.9 | 5.9 |
| Left | 21 | 3.8 | 1.74 | 7.4 | 1.6 |
| Right | 17 | 1.8 | 0.68 | 4.2 | 1.1 |
| Apple | | | | | |
| Wall | | | | | |
| Incision | 9 | 1.1 | 0.26 | 114.0 | 6.6 |
| Left | 63 | 1.8 | 1.02 | 89.0 | 18.6 |
| Right | 61 | 0.4 | 0.23 | 48.0 | 14.9 |

| | | Ratio corpus γ-max/wall γ-max Mean | SD | Max | Min |
|---|---|---|---|---|---|
| Corpus | | | | | |
| Incision | 9 | 5.7 | 0.77 | 7.5 | 4.8 |
| Left | 63 | 3.7 | 1.73 | 9.8 | 1.4 |
| Right | 61 | 2.0 | 1.32 | 7.3 | 0.8 |

[1] Relative to A-element. Max, maximum; Min, minimum.

recorded from the roof gauge were lower than or similar to those recorded from the medial orbital wall (Table 3). In experiment 8, the roof gauge averaged lower strains during mastication and incision of all foods except gelatin candies, when roof strains were consistently higher during one chewing

*TABLE 9. Descriptive statistics for experiment 41: rosette on right medial orbital wall (wall) on* Macaca *5 (female)*

| | | γ-max (με) | | | Ratio $\varepsilon_1/\lvert\varepsilon_2\rvert$ | | $\varepsilon_1$ orientation[1] | |
|---|---|---|---|---|---|---|---|---|
| Food, gauge, side | N | Mean | SD | Max | Mean | SD | Mean | SD |
| All foods | | | | | | | | |
| Wall | | | | | | | | |
| Left | 308 | 53 | 24.0 | 149 | 2.3 | 1.31 | 154 | 10.7 |
| Right | 18 | 36 | 5.5 | 50 | 0.6 | 0.31 | 145 | 2.2 |
| Prune | | | | | | | | |
| Wall | | | | | | | | |
| Left | 86 | 66 | 23.4 | 149 | 1.8 | 0.62 | 151 | 6.2 |
| Gelatin candy | | | | | | | | |
| Wall | | | | | | | | |
| Left | 30 | 83 | 16.8 | 107 | 2.7 | 0.57 | 146 | 1.2 |
| Almond | | | | | | | | |
| Wall | | | | | | | | |
| Left | 75 | 46 | 13.4 | 81 | 2.8 | 1.18 | 154 | 3.3 |
| Apricot | | | | | | | | |
| Wall | | | | | | | | |
| Left | 75 | 44 | 19.3 | 146 | 2.4 | 1.96 | 153 | 4.2 |
| Right | 18 | 36 | 5.5 | 50 | 0.6 | 0.31 | 145 | 2.2 |

[1] Relative to A-element. Max, maximum.

sequence (n = 20). In general, however, roof strains were lower than those recorded from the medial orbital wall (Table 4).

In experiments 7, 9, 29, and 45 (lower gauge), double shear strain peaks were observed. In experiment 7, mean γ-max associated with high ∠ peaks was significantly lower than that associated with low ∠ peaks; during experiment 29 the opposite was true, and during experiments 9 and 45 there was no significant difference.

### Relative timing of peak shear strains

Mandibular corpus strain patterns recorded from below $M_2$ have been shown to be good indicators of bite force magnitude and timing (Hylander, 1986). In five experiments, shear strain data were collected simultaneously from both the medial orbital wall and the mandibular corpus below the premolars, providing an opportunity to determine whether there is a consistent relationship between the timing of medial orbital wall and mandibular corpus peak shear strains. The relative timing of these two peaks was calculated simply as (time of orbital wall peak shear − time of mandibular corpus peak shear) in milliseconds (ms). A negative value indicates that the medial orbital wall shear strain peaked first, whereas a positive value indicates that the mandibular corpus values peaked first. In experiments 29 and 45, when two peaks were evident in the medial orbital wall, it was always the timing of the highest peak in the power stroke that was used.

These values are plotted in Figure 12, and descriptive statistics for these timing differences are given in Table 11. The mean differences in timing in the medial orbital wall and corpus peak shear strains are significantly different from zero in four of the experiments but are not significantly different from zero in experiment 28 on the *Otolemur*. When the data are divided by power stroke type (left, right, or incision), the mean timing of both left and right chews is significantly different from zero, but the timing differences during incision are not significantly different from zero. The temporal relationship between wall and corpus peak shear is not consistent. In some cases the significant differences involve earlier medial orbital wall peaks, and in other cases earlier mandibular corpus peaks. In 4 out of 5 experiments, mean timing of peak medial orbital wall shear strains during contralateral (left) chews precedes that during ipsilateral chews, although unpaired one-tailed *t*-tests reveal this difference to only be significant in two cases (experiments 28 and 29).

In experiments 29 and 45, where double peaks were observed in medial orbital wall gauges, timing of the high ∠ and low ∠ peaks relative to the corpus peaks were compared and found to be significantly different. In both experiments, the high ∠ peaks mostly occurred before peak loading of the mandibular corpus; the low ∠ values mostly occurred later, and often after peak strain in the mandibular corpus.

### $\epsilon_1/\lvert\epsilon_2\rvert$ ratios

Descriptive statistics of the ratio $\epsilon_1/\lvert\epsilon_2\rvert$ are given in Tables 2–10. Figure 13 plots the log of $\epsilon_1/\lvert\epsilon_2\rvert$ against the log γ-max recorded from the medial orbital wall during all experiments. Because the log of $\epsilon_1/\lvert\epsilon_2\rvert$ was used for the plots and statistical comparisons, points falling below zero (log of ratio = 1) indicate predominantly compressive strain, and points falling above zero indicate predominantly tensile strains.

Compressive strains exceed tensile strains in the majority of cases. At low strains, the $\epsilon_1/\lvert\epsilon_2\rvert$ ratio is highly variable, but as γ-max values in the medial orbital wall increase, the variability decreases. ANOVA reveals significant effects of experiment, food, and taxon on $\epsilon_1/\lvert\epsilon_2\rvert$ ratios. The $\epsilon_1/\lvert\epsilon_2\rvert$ ratios recorded during experiment 41 are unusually high. Intertaxonomic comparisons reveal that mean $\epsilon_1/\lvert\epsilon_2\rvert$ ratios are not significantly different in *Aotus*

*TABLE 10. Descriptive statistics for experiment 45: two rosettes on right medial orbital wall (upper and lower), and right mandibular corpus (corpus) of* Macaca *4*

| | | γ-max (με) | | | Ratio $\varepsilon_1/\lvert\varepsilon_2\rvert$ | | $\varepsilon_1$ orientation[1] | |
|---|---|---|---|---|---|---|---|---|
| Food, gauge, side | N | Mean | SD | Max | Mean | SD | Mean | SD |
| All foods | | | | | | | | |
| Upper | | | | | | | | |
| Incision | 2 | 25 | 3.6 | 27 | 0.1 | 0.09 | 85.0 | 1.8 |
| Left | 189 | 124 | 48.8 | 231 | 0.9 | 0.47 | 83.0 | 8.1 |
| Right | 103 | 132 | 41.6 | 204 | 0.3 | 5.20 | 81.0 | 17.5 |
| Lower | | | | | | | | |
| Incision | 2 | 83 | 18.3 | 96 | 1.0 | 0.08 | 119.0 | 1.6 |
| Left (low ∠)[2] | 53 | 265 | 124.3 | 491 | 0.7 | 0.21 | 38.0 | 5.0 |
| Left (high ∠)[2] | 136 | 262 | 121.4 | 657 | 3.1 | 0.94 | 103.0 | 6.9 |
| Right (low ∠)[2] | 71 | 174 | 45.3 | 310 | 0.8 | 0.21 | 41.0 | 6.8 |
| Right (high ∠)[2] | 29 | 154 | 54.9 | 269 | 3.5 | 1.47 | 101.0 | 5.0 |
| | | | | | Ratio corpus γ-max/upper wall γ-max | | | |
| | | | | | Mean | SD | Max | Min |
| Corpus | | | | | | | | |
| Incision | 2 | 397 | 36.8 | 423 | 16.5 | 3.90 | 19.2 | 13.7 |
| Left | 189 | 447 | 157.2 | 985 | 4.9 | 4.74 | 30.0 | 1.5 |
| Right | 103 | 354 | 97.9 | 542 | 2.8 | 0.98 | 6.7 | 1.4 |
| | | | | | Ratio corpus γ-max/lower wall γ-max | | | |
| | | | | | Mean | SD | Max | Min |
| Corpus | | | | | | | | |
| Incision | 2 | 397 | 36.8 | 423 | 4.8 | 0.62 | 5.3 | 4.4 |
| Left (low ∠)[2] | 53 | 371 | 69.1 | 537 | 1.8 | 1.17 | 7.0 | 0.7 |
| Left (high ∠)[2] | 136 | 476 | 172.1 | 985 | 2.0 | 0.85 | 6.3 | 0.7 |
| Right (low ∠)[2] | 71 | 352 | 66.9 | 468 | 2.1 | 0.45 | 3.4 | 1.4 |
| Right (high ∠)[2] | 29 | 379 | 140.3 | 542 | 2.5 | 0.48 | 3.4 | 1.5 |
| Gelatin candy | | | | | | | | |
| Upper | | | | | | | | |
| Left | 37 | 139 | 33.2 | 206 | 0.7 | 0.12 | 84.0 | 2.3 |
| Right | 39 | 163 | 26.7 | 204 | 0.6 | 0.08 | 84.0 | 14.8 |
| Lower | | | | | | | | |
| Left (low ∠)[2] | 17 | 157 | 47.5 | 245 | 0.9 | 0.30 | 43.0 | 6.4 |
| Left (high ∠)[2] | 21 | 196 | 46.0 | 265 | 2.9 | 0.53 | 97.0 | 3.4 |
| Right (low ∠)[2] | 39 | 197 | 38.6 | 310 | 0.7 | 0.19 | 37.0 | 6.2 |
| | | | | | Ratio corpus γ-max/upper wall γ-max | | | |
| | | | | | Mean | SD | Max | Min |
| Corpus | | | | | | | | |
| Left | 38 | 405 | 84.5 | 592 | 3.1 | 1.17 | 6.8 | 1.5 |
| Right | 39 | 369 | 58.7 | 469 | 2.3 | 0.46 | 3.3 | 1.4 |
| | | | | | Ratio corpus γ-max/lower wall γ-max | | | |
| | | | | | Mean | SD | Max | Min |
| Corpus | | | | | | | | |
| Left | 38 | | | | 2.5 | 1.10 | 7.0 | 1.5 |
| Right | 39 | | | | 1.9 | 0.39 | 3.1 | 1.4 |
| Prune | | | | | | | | |
| Upper | | | | | | | | |
| Incision | 2 | 25 | 3.6 | 27 | 0.1 | 0.08 | 85.0 | 1.8 |
| Left | 69 | 87 | 36.7 | 167 | 1.1 | 0.65 | 82.0 | 6.7 |
| Right | 8 | 39 | 34.0 | 120 | 1.0 | 0.31 | 90.0 | 3.5 |
| Lower | | | | | | | | |
| Incision | 2 | 83 | 18.3 | 96 | 1.0 | 0.08 | 119.0 | 1.6 |
| Left (high ∠)[2] | 69 | 320 | 139.7 | 657 | 3.4 | 0.94 | 106.0 | 7.4 |
| Right (high ∠)[2] | 6 | 85 | 14.8 | 108 | 1.2 | 0.58 | 99.0 | 9.8 |
| | | | | | Ratio corpus γ-max/upper wall γ-max | | | |
| | | | | | Mean | SD | Max | Min |
| Corpus | | | | | | | | |
| Incision | 2 | 397 | 36.8 | 423 | 16.5 | 3.90 | 19.2 | 13.7 |
| Left | 69 | 531 | 195.6 | 985 | 8.1 | 6.47 | 30.0 | 1.6 |
| Right | 6 | 171 | 24.9 | 203 | 4.9 | 2.09 | 6.7 | 1.4 |

*(continued)*

*TABLE 10. (Continued)*

| Food, gauge, side | N | γ-max (με) Mean | γ-max (με) SD | γ-max (με) Max | Ratio $\varepsilon_1/\lvert\varepsilon_2\rvert$ Mean | Ratio $\varepsilon_1/\lvert\varepsilon_2\rvert$ SD | $\varepsilon_1$ orientation[1] Mean | $\varepsilon_1$ orientation[1] SD |
|---|---|---|---|---|---|---|---|---|
| | | | | | Ratio corpus γ-max/lower wall γ-max | | | |
| | | | | | Mean | SD | Max | Min |
| Corpus | | | | | | | | |
| Incision | | | | | 4.8 | 0.62 | 5.3 | 4.4 |
| Left | | | | | 1.9 | 1.11 | 6.3 | 0.7 |
| Right | | | | | 2.1 | 0.44 | 2.5 | 1.5 |
| Nut | | | | | | | | |
| Upper | | | | | | | | |
| Left | 39 | 175 | 37.3 | 159 | 0.8 | 0.12 | 85.0 | 2.2 |
| Right | 40 | 131 | 16.1 | 104 | 0.8 | 0.08 | 84.0 | 2.2 |
| Lower | | | | | | | | |
| Left (low ∠)[2] | 23 | 389 | 65.2 | 491 | 0.6 | 0.02 | 36.0 | 1.0 |
| Left (high ∠)[2] | 16 | 219 | 35.8 | 294 | 3.9 | 0.81 | 103.0 | 1.5 |
| Right (low ∠)[2] | 21 | 166 | 25.7 | 204 | 0.9 | 0.16 | 46.0 | 4.2 |
| Right (high ∠)[2] | 19 | 187 | 35.3 | 269 | 4.4 | 0.61 | 102.0 | 2.5 |
| | | | | | Ratio corpus γ-max/upper wall γ-max | | | |
| | | | | | Mean | SD | Max | Min |
| Corpus | | | | | | | | |
| Left | 39 | 425 | 75.0 | 571 | 2.6 | 0.96 | 4.6 | 1.5 |
| Right | 40 | 423 | 62.6 | 542 | 3.3 | 0.44 | 4.0 | 2.4 |
| | | | | | Ratio corpus γ-max/lower wall γ-max | | | |
| | | | | | Mean | SD | Max | Min |
| Corpus | | | | | | | | |
| Left | | | | | 1.5 | 0.71 | 2.7 | 0.7 |
| Right | | | | | 2.5 | 0.48 | 3.4 | 1.8 |
| Apricot | | | | | | | | |
| Upper | | | | | | | | |
| Left | 33 | 113 | 28.9 | 166 | 0.8 | 0.39 | 83.0 | 5.3 |
| Lower | | | | | | | | |
| Left (low ∠)[2] | 3 | 132 | 14.9 | 149 | 0.8 | 0.04 | 42.0 | 2.1 |
| Left (high ∠)[2] | 30 | 200 | 67.7 | 394 | 2.3 | 0.57 | 100.0 | 5.8 |
| | | | | | Ratio corpus γ-max/upper wall γ-max | | | |
| | | | | | Mean | SD | Max | Min |
| Corpus | | | | | | | | |
| Left | 33 | 373 | 149.1 | 853 | 3.6 | 2.05 | 9.3 | 1.5 |
| | | | | | Ratio corpus γ-max/lower wall γ-max | | | |
| | | | | | Mean | SD | Max | Min |
| Corpus | | | | | | | | |
| Left | | | | | 1.9 | 0.39 | 2.7 | 1.2 |
| Apple | | | | | | | | |
| Upper | | | | | | | | |
| Left | 10 | 158 | 34.9 | 198 | 0.6 | 0.09 | 86.0 | 1.14 |
| Right | 15 | 114 | 26.6 | 154 | 0.8 | 0.31 | 82.0 | 2.70 |
| Lower | | | | | | | | |
| Left (low ∠)[2] | 10 | 203 | 60.0 | 286 | 0.7 | 0.09 | 36.0 | 2.2 |
| Right (low ∠)[2] | 11 | 107 | 18.0 | 130 | 1.1 | 0.12 | 43.0 | 3.6 |
| Right (high ∠)[2] | 4 | 101 | 10.1 | 115 | 2.6 | 0.91 | 97.0 | 1.4 |
| | | | | | Ratio corpus γ-max/upper wall γ-max | | | |
| | | | | | Mean | SD | Max | Min |
| Corpus | | | | | | | | |
| Left | 10 | 352 | 60.8 | 426 | 2.3 | 0.33 | 3.0 | 1.7 |
| Right | 15 | 244 | 32.8 | 305 | 2.3 | 0.66 | 4.0 | 1.5 |
| | | | | | Ratio corpus γ-max/lower wall γ-max | | | |
| | | | | | Mean | SD | Max | Min |
| Corpus | | | | | | | | |
| Left | 10 | | | | 1.8 | 0.36 | 2.4 | 1.2 |
| Right | 15 | | | | 2.3 | 0.31 | 3.0 | 2.0 |

[1] Relative to A-element. Max, maximum; Min, minimum.
[2] Low ∠, power strokes in which $\varepsilon_1$ orientation was less than 60°; high ∠, power strokes in which $\varepsilon_1$ orientation exceeded 80°. No angles fell between 60–80°.

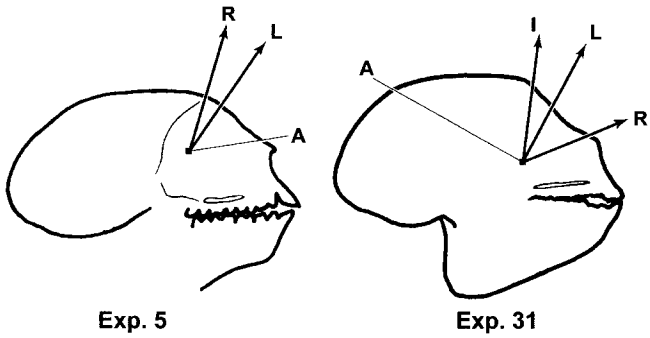


**Fig. 7.** Mean orientations of $\varepsilon_1$ relative to A-element, recorded during experiments 5 and 31 on *Aotus*. Mean orientations are given for incision (I), left chews (L), and right chews (R) across all food types in each experiment. Orientation of the A-element (A) is also given. $\varepsilon_1$ orientations are illustrated on tracings from the radiographs taken after the experiments. Arrows represent orientation only, and length of arrow is not indicative of strain magnitude.

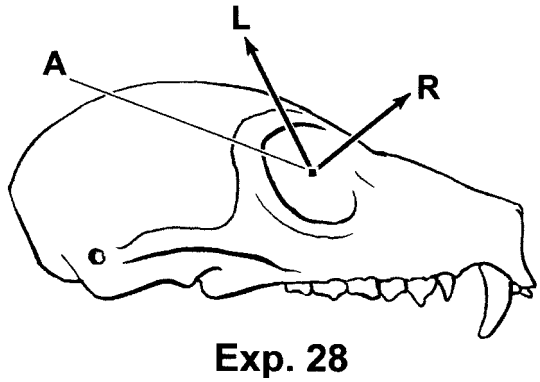


**Fig. 8.** Mean orientations of $\varepsilon_1$ relative to A-element recorded during experiment 28 on *Otolemur*. Mean orientations are given for left chews (L) and right chews (R) across all food types in the experiment. Orientation of the A-element (A) is also given. $\varepsilon_1$ orientations are illustrated on a diagram of an *Otolemur* skull. Arrows represent orientation only, and length of arrows is not indicative of strain magnitude.

and *Otolemur*, but that both taxa exhibit significantly more compressive strain along the medial orbital wall than in *Macaca*.

Unpaired one-tailed *t*-tests reveal that in 7 out of 9 experiments, the mean $\epsilon_1/|\epsilon_2|$ ratio is significantly lower during ipsilateral (right side) than contralateral (left side) chews. Five of these differences were significant at $P < 0.0001$; two were significant at $P < 0.01$. On average, across all experiments, $\epsilon_1/|\epsilon_2|$ ratios are less than zero (and compressive strains are higher) on the working side medial orbital wall, whereas $\epsilon_1/|\epsilon_2|$ ratios are greater than zero (and tensile strains are higher) on the balancing side medial orbital wall. Unpaired one-tailed *t*-tests reveal that in experiments 7, 9, 29, and 45 (lower gauge), $\epsilon_1/|\epsilon_2|$ ratios are significantly lower (indicating more compression) during high $\angle$ peaks than during low $\angle$ peaks, and in experiments 7, 9, and 29, the mean $\epsilon_1/|\epsilon_2|$ ratios are less than zero during high $\angle$ peaks and greater than zero during low $\angle$ peaks.

## DISCUSSION

The in vivo bone strain data from the medial orbital wall enable evaluation of hypotheses that: the interorbital region can be modeled as a simple beam under bending; the galago face (and that of anthropoids) is twisting on the brain case during unilateral biting or mastication (Greaves, 1985); the interorbital "pillar" is being axially compressed during incisor loading and both axially compressed and laterally bent during mastication (Endo, 1966); and the interorbital "pillar" transmits axial compressive forces from the toothrow to the braincase (Roberts and Tattersall, 1974).

### Is the primate interorbital region a bending beam?

The strain orientation and strain magnitude data reported here suggest that the anthropoid interorbital region is not behaving like an anteroposteriorly oriented beam that is bent superiorly during incision or mastication. During incision in experiments 7 and 29 on *Macaca* and 31 on *Aotus*, the orientation of $\epsilon_1$ was almost vertical relative to the palate, as predicted. However, during experiments 8, 9, and 45 on *Macaca*, $\epsilon_1$ was oriented anterosuperiorly during incision. The galago would not perform incisions. Thus, in only half of the experiments did the strain orientation data support the hypothesis that the interorbital region is bent upwards during incision.

The mastication data can only be interpreted to support the bending beam hypothesis by making some tenuous assumptions. During mastication, three loading regimes are observed. During high $\angle$ peaks in experiment 9 and low $\angle$ peaks in experiments 29 and 45 (Figs. 9, 10, 12), $\epsilon_1$ orientation is anteriorly directed. During the two *Aotus* experiments, experiment 8, and in the high $\angle$ peaks during experiments 7, 9, 29, and 45, $\epsilon_1$ orientations were anterosuperior. During experiment 41 and the low $\angle$ peaks in experiments 7 and 9 on *Macaca*, $\epsilon_1$ orientations were anteroinferior, with the experiment 41 and low $\angle$ peaks during experiment 9 close to vertical. If all the vertically oriented $\epsilon_1$ orientations came from high on the medial orbital wall, all the anterosuperior orientations came from midway down the medial orbital wall, and all the anterior orientations came from the bottom of the wall, the bending beam model would be supported. However, the highest gauges appear to have been the high medial orbital wall gauge in experiment 45 and the medial orbital wall gauge in experiment 9: The former shows consistently anterior $\epsilon_1$ orientations, whereas the latter shows anterior or inferior orientations. Moreover, in the majority of experiments, $\epsilon_1$ orientations were anterosuperior. This $\epsilon_1$ orientation should only be recorded from a bending beam on its neutral axis (Fig. 1), and not from various locations across its lateral surface, as recorded here from the medial orbital wall. Finally, the strain magnitude data reported here and elsewhere (Hylander et

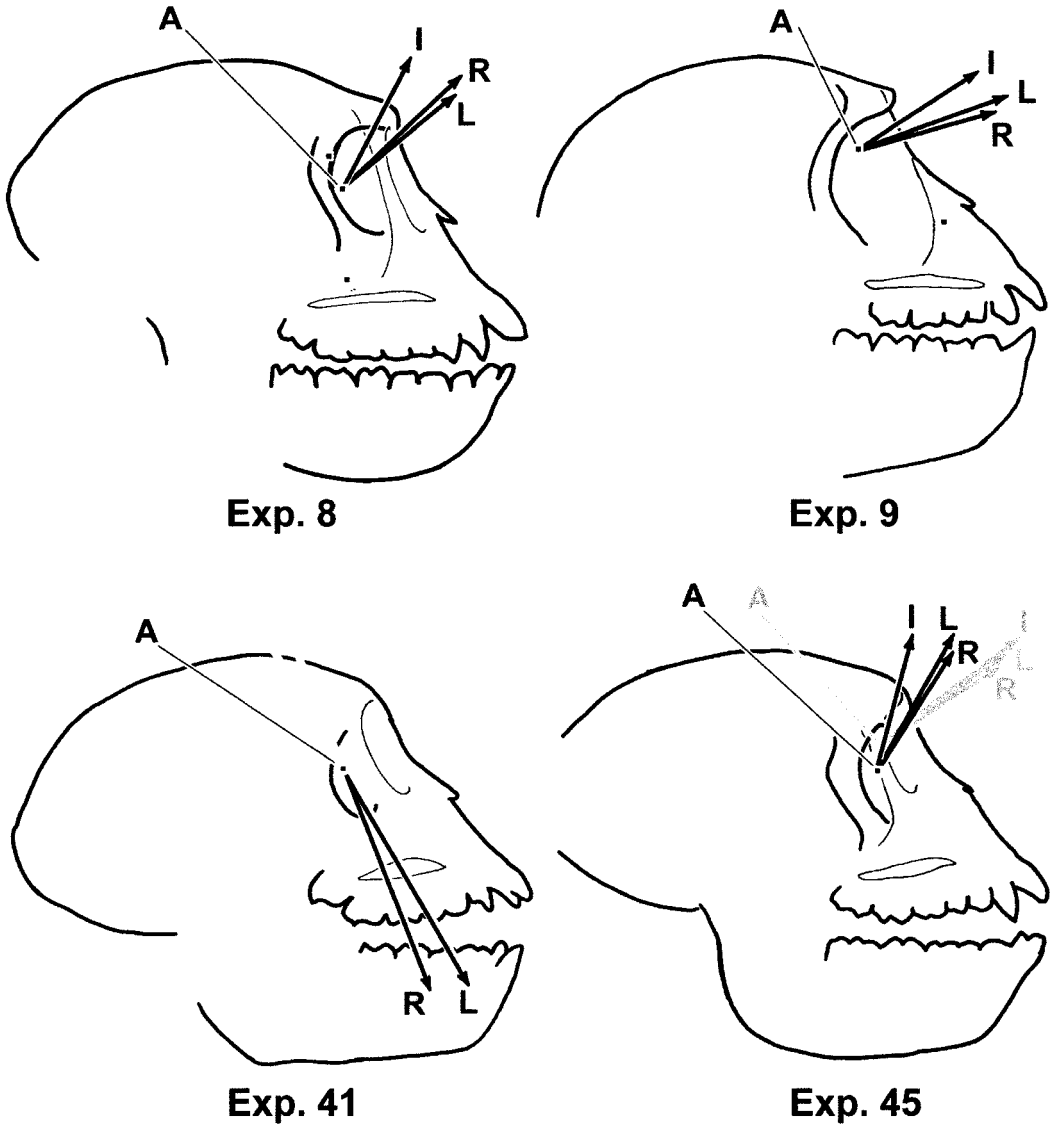


**Fig. 9.** Mean orientations of $\varepsilon_1$ relative to A-element recorded during high $\angle$ peaks. Experiments 8, 9, 41, and 45 on *Macaca.* Mean orientations are given for incision (I), left chews (L), and right chews (R) across all food types in each experiment. In experiment 45, two gauges were placed on the medial orbital wall: $\varepsilon_1$ orientations for the upper gauge are shown with gray arrows. Orientation of A-element (A) is also given. $\varepsilon_1$ orientations are illustrated on tracings from radiographs taken after experiments. For experiments 9 and 45, arrows represent mean $\varepsilon_1$ orientations for power strokes in which high values for $\varepsilon_1$ orientations were recorded. Arrows represent orientation only, and length of arrows is not indicative of strain magnitudes.

al., 1991) are lowest at the top of the skull and highest at the bottom, close to the toothrow and zygomatic arch. In a beam that is bent superiorly, strain magnitudes are highest along the top and bottom of the beam and lowest along the bending axis of neutrality, somewhere in the middle of the beam (Hibbeler, 1997).

The observed strain patterns may not match those predicted for a superiorly bending beam, because the skull is not behaving like a long beam, or it is not loaded in superiorly directed bending, or because of its complex irregular shape. It is not possible to definitively choose between these alternatives at present, but there are reasons for suggesting that superior bending in the sagittal plane is not an important loading regime in the anthropoid face during feeding. First, the moments of resistance against bending offered by the cross sections of primate rostra are not correlated with the bending moments associated with masticatory forces and forces due to gravity (Demes, 1982). Rather, the bending strengths of the skulls of *Papio* and *Gorilla* increase hyperbolically from anterior to posterior along the snout, whereas bending moments only increase linearly (Preuschoft et al., 1986). As a result, the frontal cross section of the primate skull at the level of the zygomatic arches possesses more bending strength relative to bending moments than anywhere else along the snout (see also Hylander et al., 1991).

The strength of the anthropoid face under bending in sagittal planes derives from its depth and its

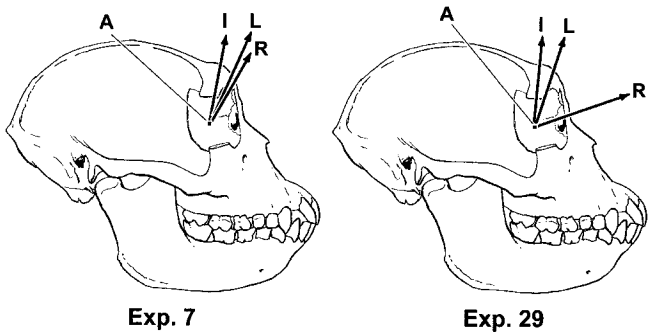


**Fig. 10.** Mean orientations of $\varepsilon_1$ relative to A-element recorded during high $\angle$ peaks during experiments 7 and 29 on *Macaca.* These data are presented separately from Figure 8, because lack of x-rays for these experiments means that A-element orientations are estimates from notes and sketches. Mean orientations are given for incision (I), left chews (L), and right chews (R) across all food types in each experiment. Orientation of A-element (A) is also given. $\varepsilon_1$ orientations are illustrated on diagrams of a skull of *Macaca.* Arrows represent mean $\varepsilon_1$ orientations for power strokes in which high values for $\varepsilon_1$ orientations were recorded. Arrows represent orientation only, and length of arrows is not indicative of strain magnitudes.

I-beam-shaped cross section (Fig. 1A). Anthropoids have very vertically deep faces, and increases in facial depth increase resistance to bending in sagittal planes by increasing the moments of area of the face perpendicular to the bending plane, something that holds true even in complexly shaped cross sections (Wainwright et al., 1982). Moreover, in the frontal plane the anthropoid circumorbital region resembles an I-beam, with the interorbital "pillar" corresponding to the vertical web, and the supraorbital torus and palate forming the upper and lower flanges. I-beams are very strong under bending because they concentrate material in the upper and lower parts of the cross section, where bending stresses are highest (Fig. 1A). Thus, the anthropoid face is probably strong under any superiorly directed bending moment acting on it during feeding (Fig. 1A).

Another possibility is that the face is so short that it behaves like a short rather than a long beam (Fig. 1C). Short beams (with a length less than four times their diameter, true of most primate faces) respond to a bending moment not by bending, but by shearing. The patterns of strain predicted in a short beam under shear are illustrated in Figure 1C: $\epsilon_1$ orientation is anterosuperior on the side of the beam. This pattern of strain matches that observed in the majority of data from the medial orbital wall of anthropoids reported here, including experiment 8, early peaks during experiments 7, and 9, and both early and late peaks during experiments 29 and 45. Two ancillary arguments can be mustered in favor of shear as an important loading regime in the anthropoid face. First, the superiorly directed components of bite force hypothesized to be acting on the anthropoid face are consistent with a shearing regime (Fig. 1). Second, the anthropoid snout also maintains a roughly constant ratio of shearing strength to shearing forces (Preuschoft et al., 1986).

However, some aspects of the in vivo bone strain data caution against concluding that shearing due to bite force is the (only) cause of the strain orientations reported here. Strain orientation data from experiment 41 and from the late peaks during experiments 7 and 9 contradict this model. Moreover, if the primary cause of strain patterns in the anthropoid medial orbital wall is superiorly directed components of bite force, as the shearing hypothesis predicts, there should be a consistent relationship between the timing of strain in the corpus and strain in the medial orbital wall, and they should not differ significantly in timing. As noted above, in the four experiments on anthropoids for which these data are available, the medial orbital wall peak shear strains occur at a different time than the corpus peak shear strain (Table 11). In addition, in four experiments the medial orbital wall exhibits two different loading regimes at different times in the power stroke, only one of which is compatible with the strain patterns predicted for dorsoventral shear. These timing differences do not exclude the possibility that the medial orbital wall is subjected to shear due to bite force, but they do suggest that this is not always the only or the most important loading regime in the medial orbital wall.

In addition, as discussed below, the anterosuperior orientation of $\epsilon_1$ observed here can also be explained with reference to Endo's rigid frame model. Consequently, it is not possible to say definitively whether the anterosuperior orientation of $\epsilon_1$ indicates shear in a structure with the cross section and material properties of an anthropoid face, although the strain orientations recorded in the majority of experiments are concordant with those predicted for a short beam under shear.

### Is the primate face a twisting cylinder?

The strain orientation data for the galago are different from those for anthropoids and suggestive of a different loading regime. The galago data are those predicted by a torsional regime in which the direction of the torsion alternates with chewing side. Torsion of a solid cylinder produces $\epsilon_1$ orientations at 45° to the long axis of the cylinder, anterosuperior in the direction of the torque (see Figs. 2, 14). Reversals in the direction of the torque produce 90° reversals in $\epsilon_1$ orientations. The in vivo data reported here (anterosuperior during ipsilateral chews and anteroinferior during contralateral chews) are consistent with torsion produced by alternating ipsilateral and contralateral torsional forces. Although the difference in $\epsilon_1$ orientation between working and balancing chews is not exactly 90°, and although these data derive from a relatively small number of power strokes from only one experiment, the conjunction of these data with data on $\epsilon_1$ orientation from the supraorbital region and the postor-

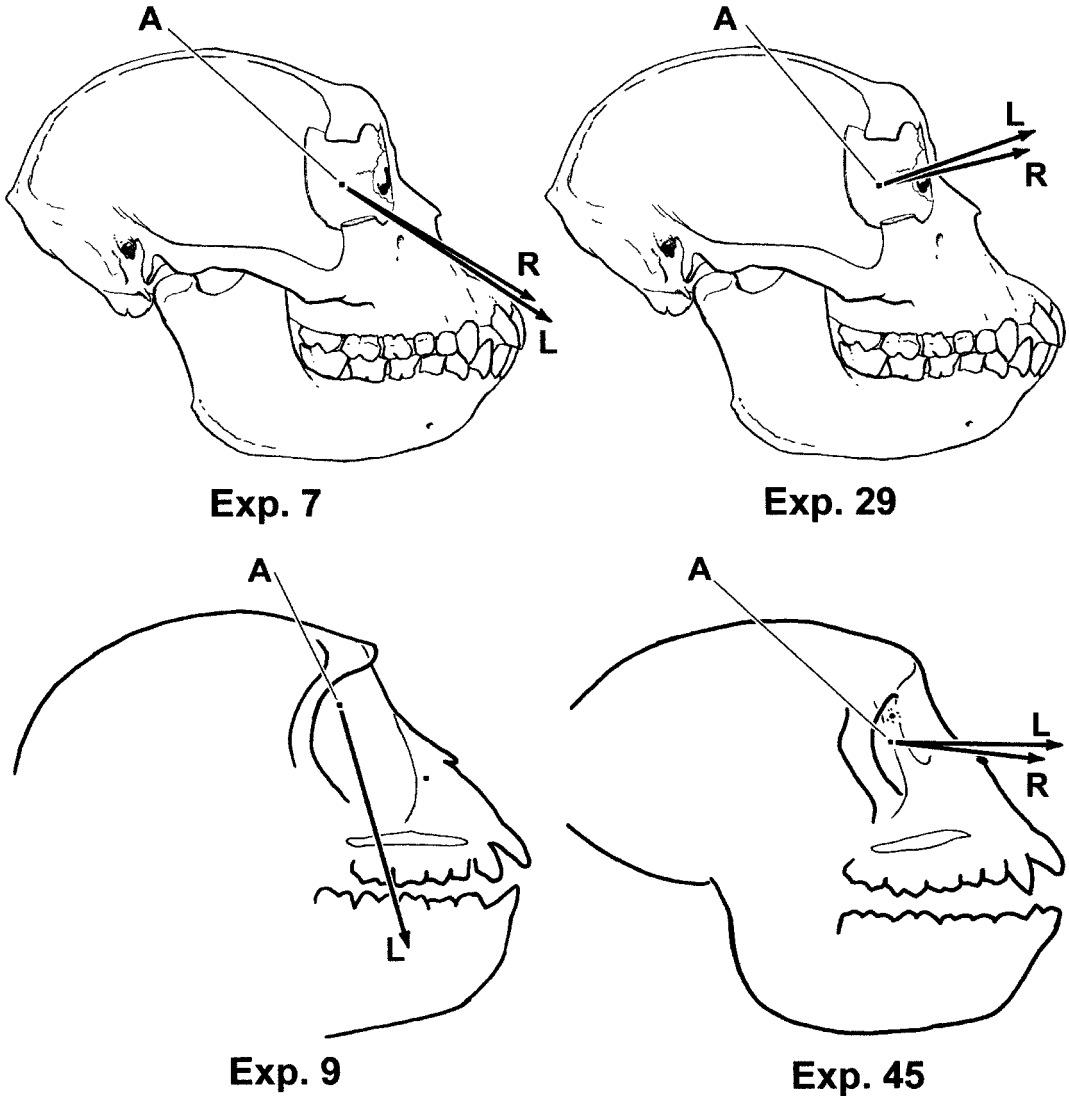


**Fig. 11.** Mean orientations of $\varepsilon_1$ relative to the A-element recorded during low $\angle$ peaks during Experiments 7, 9, 29 and 45 on *Macaca.* Mean orientations are given for left chews (L) and right chews (R) across all food types in each experiment. Orientation of the A-element (A) is also given. $\varepsilon_1$ orientations during Experiments 7 and 29 are illustrated on diagrams of a skull of *Macaca.* The arrows represent the orientation only, and the length of the arrows is not indicative of strain magnitudes.

bital bar (Ravosa et al., 2000a,b) supports torsional model of Greaves (1985).

Ravosa et al. (2000a,b) report $\epsilon_1$ orientations from the dorsal interorbital region and the lateral surface of the postorbital bar which roughly match those predicted by the twisting hypothesis of Greaves (1985). Like the data from the medial orbital wall, $\epsilon_1$ orientations along the postorbital bar and dorsal interorbital region do not change by exactly the 90° predicted by theory (Ravosa et al., 2000a,b), but they are surprisingly close, considering the irregular shape of the skull and the possibility that the orientation and position of the torsional axis may change with chewing side (Fig. 14).

In vivo research over the past decade has provided mixed support for the hypothesis of Greaves (1985). In vivo bone strain data from the postorbital bar of *Aotus* provide only mixed support for the torsion hypothesis (Ross and Hylander, 1996), and data from the supraorbital regions of macaques and baboons (Hylander et al., 1991) falsify the torsion hypothesis. Herring and Teng (2000) found torsion in the neurocranium of pigs, but attribute it to muscle contraction rather than bite force. Greaves and Mucci (1997) reported strain orientations in goats which match those predicted by the torsion hypothesis, and suggested that the configuration of the jaw muscles in primates excludes them from the twisting hypothesis. It is paradoxical that galagos now seem to support the twisting hypothesis of Greaves (1985), and it is possible that the configuration of their masticatory muscles more closely resembles that of goats than that of anthropoids.

The problem with hypothesizing that the galago skull twists during mastication but the anthropoid skull does not is that the external moments acting

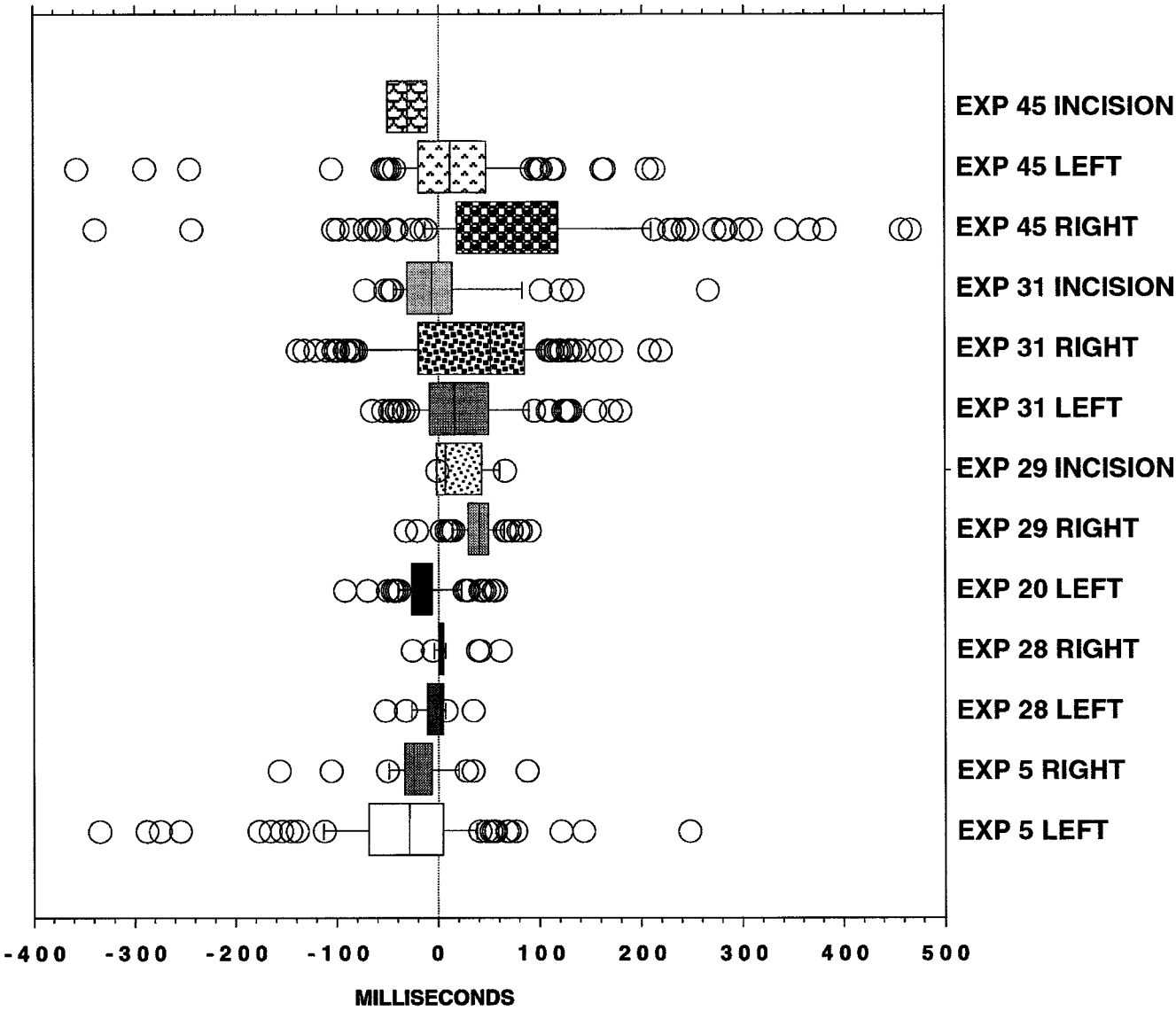


**Fig. 12.** Timing of peak shear strain in upper medial orbital wall relative to peak shear strain in corpus. Negative numbers indicate that medial orbital wall shear strains peak earlier than corpus strains. Positive numbers indicate that medial orbital wall shear strains peak later than corpus strains. Data are divided by experiment and "bite type." Line bisecting boxes indicates mean value, left and right ends of box equal 25th and 75th percentiles, respectively, and outlying lines represent 10th and 90th percentiles.

on the skulls of these two groups of primates actually predict that the strepsirrhine skull is less likely to twist during feeding than the anthropoid skull (Fig. 15). A clockwise (in Fig. 15) torsional regime is expected when the clockwise twisting moments exceed the anticlockwise twisting moments during feeding. It is well-known that in anthropoids, the ratio of working- to balancing-side muscle force is close to unity in many cases, and certainly closer to unity than in the galago, *Otolemur* (Hylander et al., 2000). Therefore, in anthropoids the torsional moments acting on the face due to balancing-side muscle force can be expected to largely cancel out the opposite torsional moments due to working-side muscle force. In anthropoids this leaves the bite force to exert a torsional moment on the facial skeleton relative to the brain case. In contrast, in *Otolemur* the ratio of working- to balancing-side muscle force during mastication is higher than unity, suggesting that during mastication the working-side muscle forces exert greater torsional moments on the face than the balancing-side muscle forces. Of course, the total torsional moment is the sum of all the torques acting in one direction minus the torques acting in the other.[3] In Figure 15, the face will twist at the craniofacial haft if ($F_{mass(b)}$ *

[3]As noted previously (Hylander et al., 1991; Ross and Hylander, 1996), when analyzing moments hypothesized to twist the face on the brain case, one need only analyze the forces acting to one side of the plane of interest, in this case the craniofacial haft. It is simplest to analyze the forces acting on the face.

*TABLE 11. Timing differences between peak shear strain in the medial orbital wall and mandibular corpus gauges*

| Experiment no. | n | Mean difference[1] | *P*-value, = 0[2] | *P*-value, LvsR[3] |
|---|---|---|---|---|
| 5, *Aotus* 3 | 159 | −34 | <0.0001 | |
| Left | 130 | −36 | <0.0001 | |
| Right | 28 | −23 | 0.005 | |
| Left vs. right | | −13 | | ns |
| 28, *Otolemur* | 54 | 1 | ns | |
| Left | 19 | −4 | ns | |
| Right | 34 | 4 | ns | |
| Left vs. right | | −8 | | 0.04 |
| 29, *Macaca* 3 | 298 | 14 | <0.0001 | |
| Left | 151 | −13 | <0.0001 | |
| Right | 13 | 38 | <0.0001 | |
| Incision | 13 | 18 | ns | |
| Left vs. right | | −52 | | <0.0001 |
| 31, *Aotus* 3 | 338 | 26 | | |
| Left | 110 | 24 | <0.0001 | |
| Right | 184 | 32 | <0.0001 | |
| Incision | 42 | 6 | ns | |
| Left vs. right | | −9 | | ns |
| 45, *Macaca* 4 | 295 | 55 | <0.0001 | |
| Left | 188 | 81 | <0.0001 | |
| Right | 99 | 12 | ns | |
| Incision | 1 | −31 | ns | |
| Left vs. right | | 68 | | ns |

[1] The relative timing of the peak shear strain in the medial orbital wall and mandibular corpus calculated as (time of orbital wall peak shear − time of mandibular corps peak shear) in msec. A negative value indicates that the medial orbital wall shear strain peaked first; a positive value indicates that the mandibular corpus values peaked first.
[2] *P*-value, for one-sample *t*-tests to determine whether mean differences in timing of peak γ-max in the medial orbital wall and mandibular corpus differed from zero; ns, not significant.
[3] *P*-value, for unpaired one-tailed *t*-tests to determine whether the relative timing of peak γ-max in the medial orbital wall occurred earlier on the balancing side (left chews) than the working side (right chews). ns, not significant.

$M_{mass(b)}$) + ($F_{bite}$ * $M_{bite}$) > ($F_{mass(w)}$ * $M_{mass(w)}$). Without knowing the relative magnitudes of these forces, it cannot be determined whether there actually is a torsional moment acting on the galago face during mastication. However, it seems more likely that the anthropoid face will be subjected to a torsional moment during mastication, given that ($F_{mass(b)}$ * $M_{mass(b)}$) and ($F_{mass(w)}$ * $M_{mass(w)}$) are close to canceling one another out. It is therefore surprising to find that the predictions of the torsional hypothesis are corroborated for *Otolemur* but not for anthropoids.

One reviewer suggested that local effects of muscle contraction might explain the presence of strain orientations concordant with the torsion hypothesis. This is indeed a possibility, as muscle contraction appears to explain the patterns of strain in the pig neurocranium during chewing (Herring and Teng, 2000). However, it seems unlikely that local effects of muscle contraction will simultaneously mimic strains due to torsion in three different parts of the galago facial skull.

Another difference between *Otolemur* and the anthropoids examined here is that similar patterns of strain occur in various places in the galago skull (the dorsal interorbital region, the postorbital bar and the medial orbital wall; Ravosa et al., 2000a,b), whereas different patterns of strain are found in different parts of anthropoid skulls (Hylander et al., 1991; Ross and Hylander, 1996). In addition, peak shear strains in the galago medial orbital wall are usually roughly coincident with peak corpus shear strains (and, by inference, bite force), but in the anthropoids the medial orbital wall strains vary in timing relative to corpus strains. Altogether, these data suggest that during feeding, the face of *Otolemur* is subjected to one single most important loading regime, in contrast with the anthropoid data which suggest different loading regimes in different parts of the face (Hylander et al., 1991; Ross and Hylander, 1996). *Aotus* and *Otolemur* are similar in skull size, suggesting that these differences in loading regimes might be due to differences in skull architecture or muscle recruitment. Anthropoids are distinguished from strepsirrhines by many such features (reviewed in Ross, 1999), but it remains to be determined which might explain these differences in strain patterns.

One possibility is that the evolution of the postorbital septum in stem haplorhines increased resistance to torques on the face (Greaves, 1985; Rosenberger, 1986), reducing or eliminating twisting as an important loading regime in anthropoids. The anthropoid skull might therefore no longer be subjected to a single predominant loading regime during feeding, instead being influenced primarily by effects of multiple loading regimes due to muscle contraction and bite force. This would imply that anthropoid and strepsirrhine facial skulls are optimized for different functions.

### Is the primate interorbital region part of a rigid frame subjected to axial compressive forces and bending moments?

On the basis of mathematical modeling and in vitro strain gauge studies on the skulls of *Gorilla* and *Homo*, Endo (1966, 1970, 1973) hypothesized that during anterior dental loading in humans and gorillas, the midline nasal member is subjected to axial compressive forces and bending moments acting in the sagittal plane. This loading regime is predicted to produce tensile strains perpendicular to the long axis of the "nasal member," i.e., anterosuperior (Fig. 4A,B). Endo (1966) also hypothesized that during loading of the posterior tooth row, the nasal member of humans and gorillas is subjected to laterally directed bending moments and axial compressive force.[4] The patterns of strain predicted by lateral bending (Fig. 4C) are anteroposterior tension on the side of the interorbital member ipsilateral to the bite point and, under pure bending, superoinferiorly oriented tension on the side of the interorbital

[4]Comparisons by Endo (1966) between stress magnitudes generated by loading different parts of the tooth row are flawed (Picq and Hylander, 1989), and are not considered here.

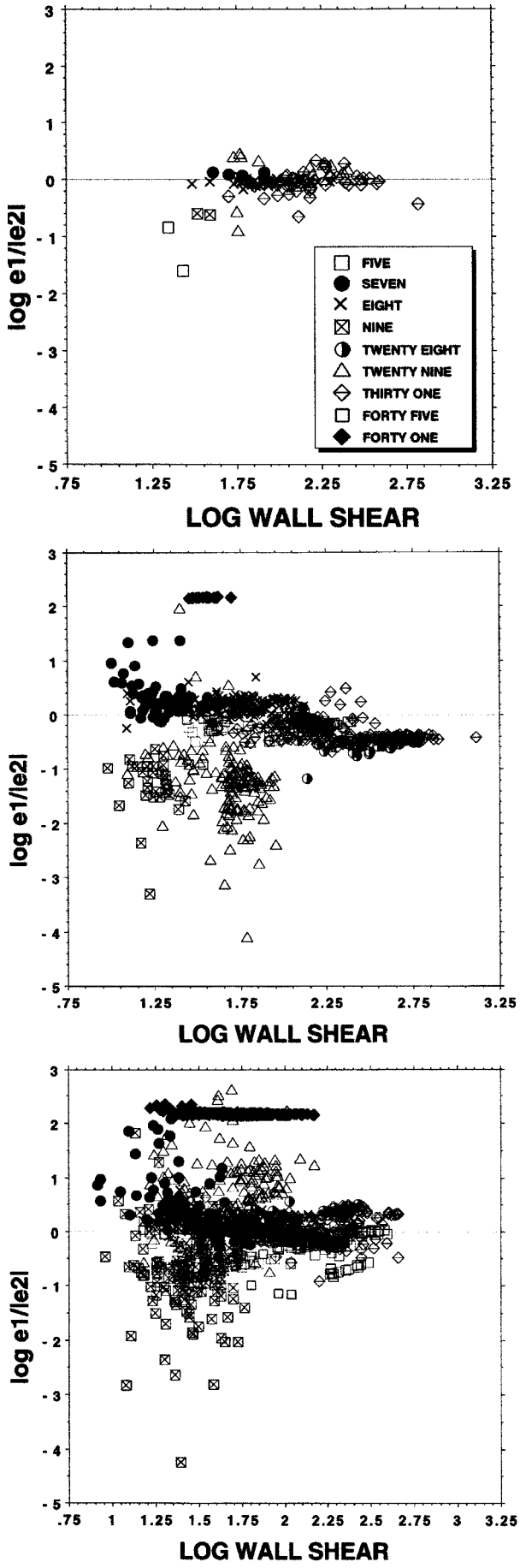


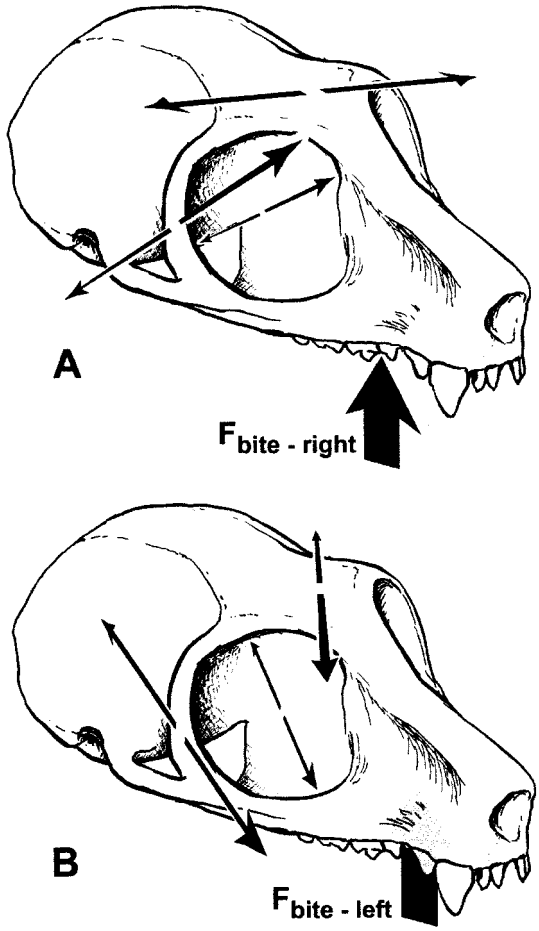


**Fig. 14.** Diagrammatic representation of maximum principal strain orientations recorded from the dorsal interorbital region and postorbital bar of *Otolemur* by Ravosa et al. (2000a,b) and from the medial orbital wall in this study. Note that $\varepsilon_1$ orientations are diagrammatic; see Ravosa et al. (2000a,b) and Figure 7 in this paper for precise data. $\varepsilon_1$ orientations do not change by exactly 90° in these studies. However, the predictions of the cylinder under torsion are fairly closely approximated.

member contralateral to the bite point. However, when this bending is combined with large axial compressive forces, strain orientations might vary from anterosuperiorly oriented tension to posterosuperiorly oriented tension, depending on the relative importance of the two loading regimes. Similarly, compressive forces on the contralateral side of the interorbital member might vary between equal to and smaller than those seen ipsilateral to the bite point. Based on in vitro studies by Endo (1966, 1970, 1973) of *Homo* and *Gorilla* skulls (Endo, 1966, his Fig. 3.6A,B), it was predicted that during mastication, the principal tensile strains will be oriented anterosuperiorly on both the ipsilateral and contralateral sides of the interorbital member (Fig. 4C),

**Fig. 13.** Bivariate plots of log $\varepsilon_1/|\varepsilon_2|$ against log $\gamma$-max recorded from the medial orbital wall during incision (top), right chews (middle), and left chews (bottom) during all experiments. Values less than zero (log of ratio = 1) indicate predominantly compression, and values greater than zero predominantly tension.

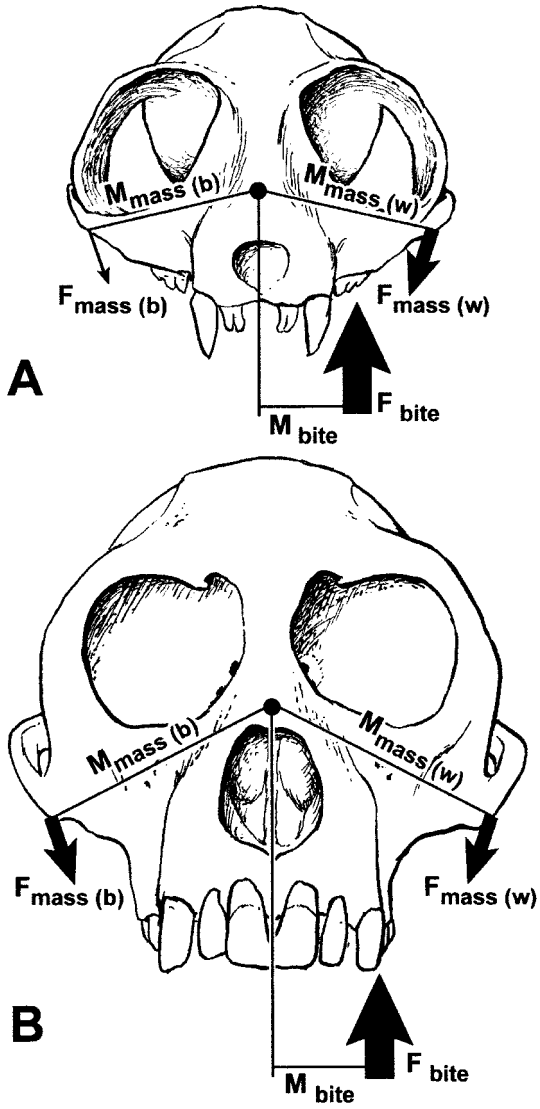


**Fig. 15.** Torques acting on the face of a strepsirrhine (*Otolemur*) and an anthropoid (*Macaca*) in anterior view. $F_{mass(b)}$, balancing side masseter muscle force; $M_{mass(b)}$, moment arm of balancing side masseter muscle force; $F_{bite}$, superiorly directed component of bite force; $M_{bite}$, moment arm of bite force; $F_{mass(w)}$, working-side masseter muscle force; $M_{mass(w)}$, moment arm of working-side masseter muscle force. Because anthropoids exhibit similar degrees of working and balancing side muscle activity during mastication, torques associated with $F_{mass(w)}$ and $F_{mass(b)}$ should roughly cancel each other out, leaving $F_{bite}$ to twist the face in a counterclockwise direction. In the strepsirrhine, balancing-side muscle activity during mastication is much lower than that on the working side, so that the face will twist in a counterclockwise direction when $(F_{mass(b)} * M_{mass(b)}) + (F_{bite} * M_{bite}) > (F_{mass(w)} * M_{mass(w)})$.

although the compressive strain will be of a smaller magnitude on the contralateral side.

The hypothesis that the interorbital region is subjected to axial compression during incision is not supported by the $\epsilon_1/|\epsilon_2|$ ratio data, and is not conclusively supported by the strain orientation data. The majority of log $\epsilon_1/|\epsilon_2|$ ratios from the medial orbital wall during incision are close to zero, and the mean log$\epsilon_1/|\epsilon_2|$ ratio does not differ significantly from zero. However, as predicted by Endo (1966), during experiments 8, 9, and 45 on *Macaca*, $\epsilon_1$ was oriented anterosuperior during incision. However, during incision in experiments 7 and 29 on *Macaca* and 31 on *Aotus*, the orientation of $\epsilon_1$ was almost vertical relative to the palate, suggesting that the interorbital "member" in these cases was not axially compressed during incision. As noted above, the galago would not perform incisions. Thus, in half of the experiments, the strain orientation data do not support the hypothesis that the interorbital region is subjected to axial compression during incision.

The hypothesis that the interorbital region is subjected to axial compression during mastication is supported by the $\epsilon_1/|\epsilon_2|$ ratio data recorded during right chews, and by the strain orientation data. During mastication, $\epsilon_1$ orientations were anterosuperior in the two *Aotus* experiments, and most *Macaca* experiments, i.e., anterosuperior during experiment 8, during high $\angle$ peaks in experiments 7, 9, 29, and 45, and during low $\angle$ peaks in experiments 29 and 45 (Figs. 9, 10, 12). The only contradictory data came from experiment 41 and the low $\angle$ peaks in experiments 7 and 9 on *Macaca*, when maximum principal (tensile) strains were oriented anteroinferior.

The hypothesis that the interorbital region is subjected to lateral bending during mastication, or rocking as suggested by Ross and Hylander (1996), is supported by the $\epsilon_1/|\epsilon_2|$ ratio data but not by the strain orientation data. The $\epsilon_1/|\epsilon_2|$ ratio data indicate that the degree of compressive strain is greater on the ipsilateral than the contralateral side, as predicted for lateral bending. However, in the macaques, strain orientations recorded during left and right chews were mostly very similar, which does not corroborate the hypothesis that the interorbital "member" is laterally bent during mastication. The only exception is the high peak values during experiment 29 (Fig. 10), when the tensile strain is more vertically oriented during chewing contralateral to the strain gauge, as predicted for lateral bending. However, in *Aotus*, where $\epsilon_1$ orientations did differ between chewing sides, those on the balancing (left) side were not consistently more vertically oriented than those on the working (right) side.

Thus, the $\epsilon_1/|\epsilon_2|$ ratio data are suggestive of some lateral bending during mastication. In contrast, the strain orientation data provide little clear signal regarding loading regimes in the interorbital region, with some data corroborating axial compression during incision and mastication and some not. The majority of the strain orientation data corroborate the hypothesis of axial compression during mastication.

### Does the primate interorbital region transmit axial compressive stresses to the brain case?

As discussed above, the $\epsilon_1/|\epsilon_2|$ ratio data from the medial orbital walls of these primates falsify the hypothesis that the interorbital region is subjected to axial compressive forces during mastication and

incision. Is the interorbital "member" transmitting any forces to the brain case? If this is the case, assuming constant cross-sectional areas and material properties from the bottom to the top of the interorbital "pillar," bone strain magnitudes should be high all the way up the interorbital "pillar," and low in the brain case. The strain values reported here reveal relatively lower bone strain magnitudes along the medial orbital wall than in the anterior root of the zygoma and the mandibular corpus, and slightly higher strains than those recorded simultaneously from the intraorbital surface of the orbital roof. Moreover, strains recorded from the lower part of the medial orbital wall were almost always higher than those recorded from the upper part of the medial orbital wall, either simultaneously, as in experiment 45 (Table 10), or during different experiments (experiment 5, upper; experiment 31, lower). These results document a gradient of decreasing strain passing up the interorbital region similar to that seen along the primate lateral orbital margin (Hylander and Johnson, 1992; Ross and Hylander, 1996, Ravosa et al., 2000b).

In vitro strain gauge studies on human and gorilla skulls by Endo (1966, 1970, 1973), and finite-element modeling of deformation of a human skull (Arbel and Hershkovitz, 2000) also suggest that strains are highest closest to the point of application of external forces and decrease with distance from these points. These data, together with the extensive in vivo strain now accumulated (Hylander and Johnson, 1992, 1997; Bouvier and Hylander, 1996; Ross and Hylander, 1996; Ravosa et al., 2000b), suggest that Saint-Venant's effects may be more important than global loading regimes in the anthropoid face during feeding (Tucker, 1954a–f, 1955a–c), and that the interorbital and lateral orbital "pillars" do not transmit stresses from the tooth row to the brain case (contra Görke, 1904; Benninghof and Goerttler, 1957; Roberts and Tattersall, 1974).

An alternate explanation for the presence of strain gradients in the primate face is that there is a single global loading regime acting. For example, during bending of a beam, strains are high on the upper and lower surfaces of the beam and lower near its bending axis. However, the timing data presented above suggest that there appears to be more than one loading regime in the medial orbital wall and that the bite force might not be the primary cause of the loading seen in the medial orbital wall. It is therefore unlikely that there is a single global loading regime of equal importance to all parts of the anthropoid face during feeding.

### What external force is producing strain in the medial orbital wall?

The existence of multiple loading regimes of the medial orbital wall associated with roughly equivalent levels of strain is suggested by the double peaks in shear strains during mastication in experiments 7, 9, 29, and 45. These two peaks are associated with two distinctly different strain environments. The high $\angle$ peaks occur prior to the peak shear strains in the mandibular corpus; are mostly associated with anterosuperior $\epsilon_1$ orientations and relatively higher compressive strains; and are mainly found on the balancing side (i.e., during left chews). The low $\angle$ peaks occur after the peak shear strain in the mandibular corpus; are associated with anteroinferior or anterior $\epsilon_1$ orientations; are associated primarily with relatively higher tensile strains; and are mainly found on the working side (i.e., during right chews).

What external forces might be producing these loading regimes? The contribution of either the medial pterygoid or the masseter muscles to the loading regime in the medial orbital wall is suggested by the fact that the high $\epsilon_1$ orientation values are usually found on the balancing side *prior* to peak shear strain in the mandibular corpus, whereas the low $\epsilon_1$ orientations values are usually associated found on the working side *after* peak shear strain in the mandibular corpus. In *Macaca fascicularis* and *Papio anubis* chewing an apple, the balancing side masseter and medial pterygoid muscles are known to reach their peak activity, on average, between 25–29 msec prior to the corresponding muscle on the working side (Hylander et al., 1992; Hylander and Johnson, 1994). The mean difference in timing between the high (early) and low (late) value peaks in experiments 29 and 45 are 50 msec and 94 msec, respectively. In the one apple-chewing sequence in experiment 45, the mean timing difference between the low $\angle$ and the high $\angle$ peak values is 30 msec, although in this sequence, the high $\angle$ and low $\angle$ peaks are not consistently associated with different chewing sides. Exactly which of these two muscles might be responsible for these double peaks cannot be determined at present. Analysis of EMG timing data in conjunction with these strain data is in progress and will be presented elsewhere.

One reviewer suggested that the double peaks seen on the medial orbital wall might be due to collapse of the food bolus during the power stroke. This hypothesis is not supported by strain patterns in the mandibular corpus: double peaks in the medial orbital wall are not always associated with double peaks or other obvious changes in loading regime in the mandibular corpus.

### Strain magnitudes and the function of the medial orbital wall

Bone strain magnitudes along the medial orbital wall are generally quite low. Mean shear strain magnitudes calculated for different activities reach only 263 $\mu\epsilon$ in *Macaca*, 319 $\mu\epsilon$ in *Aotus*, and 346 $\mu\epsilon$ in *Otolemur*. Low levels of strain were previously reported for the rostral and dorsal interorbital regions in macaques (Hylander et al., 1991), for the dorsal interorbital region in *Aotus* (Ross and Hylander, 1996), and for the dorsal interorbital region

and postorbital bar of *Otolemur* (Ravosa et al., 2000b). The combination of relatively low strain magnitudes along the medial orbital wall and the dorsal and rostral interorbital regions suggests that the interorbital "pillar" is not highly strained during incision and mastication in primates. It therefore seems unlikely that the interorbital "pillar" is specifically adapted for dissipation or transmission of feeding forces (contra Endo, 1966). Of course, the fact that the primate face remains attached to the brain case during feeding means that feeding forces must be resisted in part by the structures connecting the tooth row to the neurocranium, i.e., the interorbital "pillar," the lateral orbital wall, zygomatic arch, and the pterygoid processes. However, it does not necessarily follow that these structures are *designed* to resist these forces; i.e., that there are adaptations of shape or mass in the interorbital region for resisting feeding forces. Indeed, the low strain magnitudes reported here suggest that the interorbital region is not optimally designed to resist feeding forces, and is in fact overdesigned for this role. In support of this argument, the ability of adult *Saimiri* to resist feeding forces does not seem to be compromised by the bony fenestra in the interorbital pillar (Maier, 1983; Hartwig, 1995).

Relatively low bone strain magnitudes have also been recorded elsewhere in the circumorbital regions of cercopithecines (Hylander et al., 1991; Hylander and Johnson, 1992, 1997), owl monkeys (Ross and Hylander, 1996) and galagos (Ravosa et al., 2000b), indicating relatively high safety factors in the circumorbital skeleton. These relatively high safety factors in turn suggest that these circumorbital structures are not optimally designed to resist feeding forces, where optimality is defined as maximum strength for a minimum of material (Roux, 1881; Frost 1990; Kummer, 1972; Lanyon and Rubin, 1985). It has been hypothesized that the supraorbital torus might be optimized not to resist feeding forces, but to resist high strain magnitude traumatic loads associated with infrequent blows to the head (Hylander et al., 1991; Hylander and Ravosa, 1992; Hylander and Johnson, 1992, 1997). While this hypothesis may well apply to superficial aspects of the primate facial skeleton, it cannot explain the presence of low strain magnitudes along the medial orbital wall during mastication. The bone in this region of the face is very thin, leading to the canonical admonishment of anthropologists-in-training not to carry skulls with their fingers in the orbits! Such thin bones are unlikely to significantly augment the strength of the face either against blows to the surface or against blows that have managed to penetrate into the orbit. Clearly a function other than dissipating feeding forces or occasional trauma must be identified.

Moss (1962) recognized long ago (see also Moss and Salentijn, 1969) that the bones of the face have many functions other than dissipation of masticatory forces, and that their form will be related to the functional requirements of adjacent functional units. The thin bones forming the medial orbital wall not only form the wall of the orbit, but also the lateral wall of the posterior nasal cavity and ethmoid air sinuses, the roof of the medial aspect of the maxillary sinus, and the depression in which the olfactory lobes rest, before curving superiorly to form the floor of the anterior cranial fossa. It is suggested that the bones forming the lateral wall of the nasal cavity and roof of the maxillary sinus provide a rigid support not only for the respiratory and olfactory epithelium of these spaces, but also for the eye, the extraocular muscles, and the complex connective tissue septa that Koorneef (1977, 1992) found attaching the extraocular muscles to the bony orbit. The presence of rigid bone between the orbits might also be argued to prevent eye movements in one orbit from disturbing the contralateral eye, although *Saimiri* possesses both an interorbital fenestra and apparently normal visual abilities. The bones flooring the anterior cranial fossa and walling the fossa for the olfactory bulbs provide a rigid support for the brain and its meninges (Ross, 1999). The postorbital septum of tarsiers and anthropoids deflects the chewing muscles around the orbital contents, while that of most catarrhines also provides attachment for temporalis and zygomaticomandibularis muscles (Ross, 1995). Any role that these thin circumorbital bony plates perform in resisting feeding forces is coincidental and insignificant, and could be better performed by a more efficient distribution of bony tissue (Ross and Hylander, 1996).

## CONCLUSIONS

The precise nature of the loading regimes in the medial orbital wall is not clear. The interorbital region cannot be modeled as a anteroposteriorly oriented beam bent superiorly in the sagittal plane during incision or mastication. The strain orientations recorded in the majority of experiments are concordant with those predicted for a short beam under shear, but the external forces producing this loading regime are not identified. The hypothesis that the strepsirrhine face is twisted during mastication is corroborated by predicted by the bone strain data presented here and elsewhere (Ravosa et al, 2000a, b). The hypothesis that the interorbital region is part of a rigid frame subjected to axial compression during mastication is supported by the $\epsilon_1/|\epsilon_2|$ ratio data recorded during right chews, and to some degree by the strain orientation data. The hypothesis that during mastication the interorbital region is a rigid frame subjected to lateral bending as suggested by Endo (1966), or rocking as suggested by Ross and Hylander (1996), is supported by the $\epsilon_1/|\epsilon_2|$ ratio data but not by the strain orientation data.

Low strain magnitudes and variable loading regimes in the medial orbital wall suggest that the morphology of the anthropoid interorbital region is unlikely to be specifically adapted for resisting

forces generated during feeding (i.e., mastication and incision). Variation in interorbital morphology among anthropoids is therefore unlikely to be related to masticatory function. In *Otolemur*, the strain magnitudes in the medial orbital wall are also relatively low but there is some evidence for a torsional loading regime in the circumorbital region. Low strain magnitudes in the thin bony plates surrounding the orbit suggest that they are not adapted for resisting forces generated in the face during feeding. It is suggested that these thin bony plates rather function to provide rigid support and protection for soft tissue structures, a function that can be achieved with a minimum of material. Strain gradients evident in the primate face suggest that feeding forces may be important close to their point of application, but of decreasing importance with increasing distance from then point of application. Rigid framework models of the face (e.g., Endo, 1966) do not accurately reflect this situation. These results have significant implications for definitions of the masticatory apparatus, hypotheses of functional integration in the skull and the use of craniofacial features in phylogeny reconstruction. The bony masticatory apparatus might be defined as that part of the skull that suffers high strains during mastication, with decreasing strains indicating decreased participation in the masticatory system. Similarly, those parts of the face suffering high strains during mastication might be expected to covary in measures relevant to their biomechanical strength under masticatory loads. If this turns out to be so, these covarying elements might not be independent elements form parsimony approaches to phylogeny reconstruction (e.g., Skelton and McHenry, 1992).

## ACKNOWLEDGMENTS

This research was greatly facilitated by the expert assistance and support of the experimentalists at Stony Brook: Brigitte Demes, Susan Larson, and Jack Stern. Kristin Fuehrer and three graduate students, Rob Asher, Chris Heesy, and Keith Metzger, ably assisted with animal training, preparation, and surgeries. Mitchell Irwin assisted with preparation of the manuscript. Division of Laboratory Animal Resources veterinarians and technicians provided expert assistance with anesthesia, surgery and animal handling. Brigitte Demes, Sue Herring, and four anonymous reviewers provided insightful comments on the manuscript.

## LITERATURE CITED

Arbel G, Hershkovitz I. 2000. Strain distributions on the skull due to occlusal loading: An anthropological perspective. Homo 51:30–55.

Benninghof A. Goerttler K. 1957. Lehrbuch der Anatomie des Menschen. Munich.

Borrazo EC, Hylander WL, Rubin CT. 1994. Validation of a finite-element model of the functionally loaded zygomatic arch by in vivo strain gage data. Proc Am Soc Biomech 18:51–52.

Bluntschli H. 1926. Rückwirkung des Kieferapparatus auf den Gesamtschädel. Z Zahnartztl Orthoped 18:57–79.

Bouvier M, Hylander WL. 1996. Strain gradients, age, and levels of modeling and remodeling in the facial bones of *Macaca fascicularis*. In: Davidovitch Z, Norton LA, editors. Biological mechanisms of tooth movement and craniofacial adaptation. Boston: Harvard Society for the Advancement of Orthodontics. p 407–412.

Cartmill M. 1974. *Daubentonia*, *Dactylopsila*, woodpeckers and klinorhynchy. In: Martin RD, Doyle GA, Walker AC, editors. Prosimian biology. London: Duckworth. p 655–670.

Chen X. 1995. Biomechanics of the hominoid masticatory apparatus. Ph.D. dissertation, Yale University, New Haven, Connecticut.

Connolly R, Quimby FW. 1978. Acepromazine-ketamine anesthesia in the rhesus monkey (*Macaca mulatta*). Lab Anim Sci 28:72–74.

Couly G. 1976. La statique osseuse de la face. Rev Stomatol 77:420–426.

Dally JW, Riley WF. 1965. Experimental stress analysis. New York: McGraw Hill.

Dechow P, Nail GA, Schwartz-Dabney CL, Ashman, RB. 1993. Elastic properties of human supraorbital and mandibular bone. Am J Phys Anthropol 90:291–306.

Demes B. 1982. The resistance of primate skulls against mechanical stresses. J Hum Evol 11:687–691.

Endo B. 1966. Experimental studies on the mechanical significance of the form of the human facial skeleton. J Facult Sci Univ Tokyo [V] 3:1–106.

Endo B. 1970. Analysis of stresses around the orbit due to masseter and temporalis muscles respectively. J Anthrop Soc Nippon 78:251–266.

Endo B. 1973. Stress analysis on the facial skeleton of gorilla by means of the wire strain gauge method. Primates 14:37–45.

Frost HM. 1990. Skeletal structural adaptations to mechanical usage (SATMU): 1. Redefining Wolff's law: the bone modeling problem. Anat Rec 226:403–413.

Frazzetta TH. 1962. A functional consideration of cranial kinesis in lizards. J Morphol 111:287–320.

Görke O. 1904. Beitrag zur funktionellen Gestaltung des Schädels bei den Anthropomorphen und Menschen durch Untersuchung mit Röntgenstrahlen. Arch Anthrop 1:91–108.

Greaves WS. 1985. The mammalian postorbital bar as a torsion-resisting helical strut. J Zool (Lond) 207:125–136.

Greaves WS. 1995. Functional predictions from theoretical models of the skull and jaws in reptiles and mammals. In: Thomason JJ, editor. Functional morphology in vertebrate paleontology. New York: Cambridge University Press. p 99–115.

Greaves WS, Mucci RJ. 1997. Mechanical loads in the postorbital bar during mastication in artiodactyls and primates. Am J Phys Anthropol [Suppl] 23:119.

Hartwig WC. 1995. Effect of life history on the squirrel monkey (Plattyrrhini, *Saimiri*) cranium. Am J Phys Anthropol 97:435–449.

Herring SW, Mucci RJ. 1991. In vivo strain in cranial sutures: the zygomatic arch. J Morphol 207:225–239.

Herring SW, Teng S. 2000. Strain in the braincase and its sutures during function. Am J Phys Anthropol 112:575–593.

Herring SW, Teng S, Huang X, Mucci RJ, Freeman J. 1996. Patterns of bone strain in the zygomatic arch. Anat Rec 246: 446–457.

Hibbeler RC. 1997. Mechanics of materials. 3rd ed. Upper Saddle River, NJ: Prentice Hall.

Hylander WL. 1972. The adaptive significance of Eskimo craniofacial morphology. Ph.D. dissertation, University of Chicago.

Hylander WL. 1977. The adaptive significance of Eskimo craniofacial morphology. In: Dahlberg AA, Graber TM, editors. Orofacial growth and development. The Hague: Mouton. p 129–169.

Hylander WL. 1979a. Mandibular function in *Galago crassicaudatus* and *Macaca fascicularis*: an in vivo approach to stress analysis of the mandible. J Morphol 159:253–296.

Hylander WL. 1979b. The functional significance of primate mandibular form. J Morphol 160:223–239.

Hylander WL. 1981. Patterns of stress and strain in the macaque mandible. In: Carlson DS, editor. Craniofacial biology. Mono-

graph #10. Craniofacial growth series. Center for Human Growth and Development. Ann Arbor: University of Michigan. p 1–37.
Hylander WL. 1985. Mandibular function and biomechanical stress and scaling. Am Zool 25:315–330.
Hylander WL. 1986. *In vivo* bone strain as an indicator of masticatory bite force in *Macaca fascicularis*. Arch Oral Biol 31: 149–157.
Hylander WL, Johnson KR. 1989. The relationship between masseter force and masseter electromyogram during mastication in the monkey *Macaca fascicularis*. Arch Oral Biol 34:713–722.
Hylander WL, Johnson KR. 1992. Strain gradients in the craniofacial region of primates. In: Davidovich Z, editor. The biological mechanisms of tooth movement and craniofacial adaptation. Columbus, OH: Ohio State University. p 559–569.
Hylander WL, Johnson KR. 1994. Jaw muscle function and wishboning of the mandible during mastication in macaques and baboons. Am J Phys Anthropol 94:523–547.
Hylander WL, Johnson KR. 1997. *In vivo* bone strain patterns in the craniofacial region of primates. In: McNeill C, editor. Science and practice of occlusion. Chicago: Quintessence Publishing Co. p 165–178.
Hylander WL, Picq PG, Johnson KR. 1991. Masticatory-stress hypotheses and the supraorbital region of primates. Am J Phys Anthropol 86:1–36.
Hylander WL, Johnson KR, Crompton AW. 1992. Muscle force recruitment and biomechanical modeling: an analysis of masseter muscle function during mastication in *Macaca fascicularis*. Am J Phys Anthropol 88:365–387.
Hylander WL, Ravosa MJ, Ross CF, Wall CE, Johnson KR. 2000. Symphyseal fusion and jaw-adductor muscle force: an EMG study. Am J Phys Anthropol 112:469–492.
Jaslow CR. 1990. Mechanical properties of cranial sutures. J Biomech 23:313–321.
Koornneef L. 1977. New insights in the human orbital connective tissue. Arch Opthalmol 95:1269–1273.
Koornneef L. 1992. Orbital connective tissue. In: Tasma W, editor. Duane's foundations of clinical ophthalmology, volume 1. Philadelphia: J.S. Lippincott Co. p 1–23.
Kummer BKF. 1972. Biomechanics of bone: mechanical properties, functional structure, functional adaptation. In: Fung YC, Proone N, Anlicker M, editors. Biomechanics—its foundations and objectives. Englewood Cliffs, NJ: Prentice-Hall Inc. p 237–271.
Lanyon LE, Rubin CT. 1985. Functional adaptation in skeletal structures. In: Hildebrand M, Bramble DM, Liem KF, Wake DB, editors. Functional vertebrate morphology. Cambridge, MA: Harvard University Press. p 1–25.
Maier W. 1983. Morphology of the interorbital region of *Saimiri sciureus*. Folia Primatol (Basel) 41: 277–303.
Moss ML. 1962. The functional matrix. In: Kraus B, Reidel R. Vistas in orthodontics. Philadelphia: Lea and Febiger. p 85–98.
Moss ML, Salentijn L. 1969. The primary role of functional matrices in facial growth. Am J Orthod 55:566–577.
Picq PG, Hylander WL. 1989. Endo's stress analysis of the primate skull and the functional significance of the supraorbital region. Am J Phys Anthropol 79:393–398.
Preuschoft H, Demes B, Meyer M, Bar HF. 1986. The biomechanical principles realised in the upper jaw of long-snouted primates. In: Else JG, Lee PC, editors. Primate evolution. Cambridge: Cambridge University Press. p 249–264.
Rafferty KL, Herring SW. 2000. Craniofacial sutures: morphology, growth and in vivo masticatory strains. J Morphol 242: 167–179.
Rak Y. 1983. The australopithecine face. New York: Academic Press.
Rak Y. 1986. The Neanderthal: a new look at an old face. J Hum Evol 14:151–164.
Ravosa MJ. 1988. Browridge development in Cercopithecidae: a test of two models. Am J Phys Anthropol 76:535–555.
Ravosa MJ. 1991. Ontogenetic perspective on mechanical and nonmechanical models of primate circumorbital morphology. Am J Phys Anthropol 85:95–112.
Ravosa MJ, Noble VE, Hylander WL, Johnson KR, Kowalski EM. 2000a. Masticatory stress, orbital orientation and the evolution of the primate postorbital bar. J Hum Evol 38:667–693.
Ravosa MJ, Johnson KR, Hylander WL. 2000b. Strain in the galago facial skull. J Morphol 245:51–66.
Richter W. 1920. Der Obergesichtschädel des Menschen als Gebissturm, ein Statische Kunstwerk. Dtsch Monatsschr Zahnheilkd 38:49–68.
Roark RJ, Young WC. 1975. Formulas for stress and strain, 5th ed. New York: McGraw-Hill.
Roberts D, Tattersall I. 1974. Skull form and the mechanics of mandibular elevation in mammals. Am Mus Novit 2536:1–9.
Rosenberger AL. 1986. Platyrrhines, catarrhines and the anthropoid transition. In: Wood B, Mantin L, Andrews P, editors. Topics in primate and human evolution. Cambridge: Cambridge University Press. p 66–88.
Ross CF. 1995. Muscular and osseous anatomy of the primate anterior temporal fossa and the functions of the postorbital septum. Am J Phys Anthropol 98:275–306.
Ross CF. 1999. In vivo intraorbital bone strain in anthropoid primates during mastication and incision. Am J Phys Anthropol [Suppl] 28:236.
Ross CF, Chen X. 1997. A finite element model of the owl monkey circumorbital region: comparison with in vivo and in vitro bone strain data. Am J Phys Anthropol [Suppl] 23:200.
Ross CF, Hylander WL. 1996. In vivo and in vitro bone strain in the owl monkey circumorbital region and the function of the postorbital septum. Am J Phys Anthropol 101:183–215.
Roux W. 1881. Der Kampf der Theile in Organismus. Leipzig: Engelmann.
Russell AP, Thomason JJ. 1993. Mechanical analysis of the mammalian head skeleton. In: Hanken J, Hall BK, editors. The skull. Volume 3: Functional and evolutionary mechanisms. Chicago: Chicago University Press. p 345–383.
Sicher H, Tandler J. 1928. Anatomie für Zahnärtzte. Berlin: Springer.
Schwenk K. 2000. An introduction to tetrapod feeding. In: Schwenk K, editor. Feeding. New York: Academic Press. p 21–61.
Skelton RR, McHenry HM. 1992. Evolutionary relationships among early hominids. J Hum Evol 23:309–349.
Thomason JJ, Russell AP. 1986. Mechanical factors in the evolution of the mammalian secondary palate: a theoretical analysis. J Morphol 189:199–213.
Tucker R. 1954a. Studies in functional and analytical craniology. I. The elements of analysis. Austr. J. Zool. 2: 381-390.
Tucker R. 1954b. Studies in functional and analytical craniology. II. The functional classification of mammalian skulls. Austr. J. Zool. 2: 391-398.
Tucker R. 1954c. Studies in functional and analytical craniology. III. The breviarcuate skull and its analysis. Austr. J. Zool. 2: 399-411.
Tucker R. 1954d. Studies in functional and analytical craniology. IV. More extreme forms of the breviarcuate skull. Austr. J. Zool. 2: 412-417.
Tucker R. 1954e. Studies in functional and analytical craniology. V. The functional metamorphoses of the carnivorous skull. Austr. J. Zool. 2: 418-426.
Tucker R. 1954f. Studies in functional and analytical craniology. VI. Strains and the direction of certain vectors in the breviarcuate skull. Austr. J. Zool. 2: 427-430.
Tucker R. 1955a. Studies in functional and analytical craniology. VII. The longoarcuate skull. Aust J Zool 3:513–522.
Tucker R. 1955b. Studies in functional and analytical craniology. VIII. The planoarcuate skull. Aust J Zool 3:523–529.
Tucker R. 1955c. Studies in functional and analytical craniology. IX. The comparative evolutional outlook. Aust J Zool 3:530–540.
Wainwright SA. Biggs WD, Currey JD, Gosline JM. 1982. Mechanical design in Organisms. Princeton: Princeton University Press.
Zusi R. 1984. A functional and evolutionary analysis of rhynchokinesis in birds. Smithson Contrib Zool 395:1–40.